Research Article

Cortical transcriptome analysis after spinal cord injury reveals the regenerative mechanism of central nervous system in CRMP2 knock-in mice

https://doi.org/10.4103/1673-5374.301035
Date of submission: June 29, 2020
Date of decision: September 8, 2020
Date of acceptance: October 10, 2020
Date of web publication: December 12, 2020

Ayaka Sugeno[1, 3], Wenhui Piao[1], Miki Yamazaki[2, 3], Kiyofumi Takahashi[4], Koji Arikawa[4], Hiroko Matsunaga[4], Masahito Hosokawa[2, 4, 5], Daisuke Tominaga[3, 6], Yoshio Goshima[7], Haruko Takeyama[2, 3, 4, 5], Toshio Ohshima[1, 5, *]

Graphical Abstract *CRMP2 knock-in induces structural recovery in the cortex and has characteristic mRNA profile after spinal cord injury*

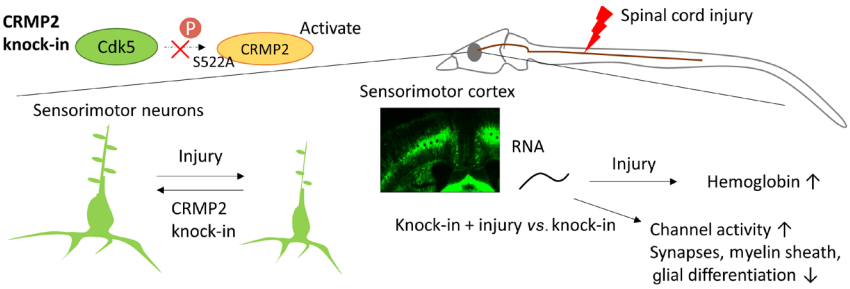

Abstract

Recent studies have shown that mutation at Ser522 causes inhibition of collapsin response mediator protein 2 (CRMP2) phosphorylation and induces axon elongation and partial recovery of the lost sensorimotor function after spinal cord injury (SCI). We aimed to reveal the intracellular mechanism in axotomized neurons in the CRMP2 knock-in (CRMP2KI) mouse model by performing transcriptome analysis in mouse sensorimotor cortex using micro-dissection punching system. Prior to that, we analyzed the structural pathophysiology in axotomized or neighboring neurons after SCI and found that somatic atrophy and dendritic spine reduction in sensorimotor cortex were suppressed in CRMP2KI mice. Further analysis of the transcriptome has aided in the identification of four hemoglobin genes Hba-a1, Hba-a2, Hbb-bs, and Hbb-bt that are significantly upregulated in wild-type mice with concomitant upregulation of genes involved in the oxidative phosphorylation and ribosomal pathways after SCI. However, we observed substantial upregulation in channel activity genes and downregulation of genes regulating vesicles, synaptic function, glial cell differentiation in CRMP2KI mice. Moreover, the transcriptome profile of CRMP2KI mice has been discussed wherein energy metabolism and neuronal pathways were found to be differentially regulated. Our results showed that CRMP2KI mice displayed improved SCI pathophysiology not only via microtubule stabilization in neurons, but also possibly via the whole metabolic system in the central nervous system, response changes in glial cells, and synapses. Taken together, we reveal new insights on SCI pathophysiology and the regenerative mechanism of central nervous system by the inhibition of CRMP2 phosphorylation at Ser522. All these experiments were performed in accordance with the guidelines of the Institutional Animal Care and Use Committee at Waseda University, Japan (2017-A027 approved on March 21, 2017; 2018-A003 approved on March 25, 2018; 2019-A026 approved on March 25, 2019).
Key Words: CNS regeneration; cortex; CRMP2; hemoglobin; metabolic pathway; spinal cord injury; spine; transcriptome

Chinese Library Classification No. R459.9; R364; R741

Introduction

Mammalian central nervous system (CNS) has limited ability to regenerate and recover after injury. Spinal cord injury (SCI) is one such typical injury which is characterized by its semi-permanent impairments in sensorimotor functions below the spinal cord lesion. Though new treatment regimen for SCI by stem cell transplantation is gradually developing (Nakamura and Okano, 2013), promising approach for regenerating CNS

[1]Laboratory for Molecular Brain Science, Department of Life Science and Medical Bioscience, Graduate School of Advanced Science and Engineering, Waseda University, Tokyo, Japan; [2]Biomolecular Engineering Laboratory, Department of Life Science and Medical Bioscience, Graduate School of Advanced Science and Engineering, Waseda University, Tokyo, Japan; [3]Computational Bio Big-Data Open Innovation Laboratory (CBBD-OIL), National Institute of Advanced Industrial Science and Technology (AIST), Tokyo, Japan; [4]Research Organization for Nano and Life Innovation, Waseda University, Tokyo, Japan; [5]Institute for Advanced Research of Biosystem Dynamics, Waseda Research Institute for Science and Engineering, Graduate School of Advanced Science and Engineering, Waseda University, Tokyo, Japan; [6]Cellular and Molecular Biotechnology Research Institute, National Institute of Advanced Industrial Science and Technology (AIST), Tsukuba, Japan; [7]Department of Molecular Pharmacology and Neurobiology, Graduate School of Medicine, Yokohama City University, Yokohama, Japan
***Correspondence to:** Toshio Ohshima, MD, PhD, ohshima@waseda.jp.
https://orcid.org/0000-0003-4931-7087 (Toshio Ohshima)

Funding: *This work was supported by Grants-in-Aid for Scientific Research on Priority Areas from The Ministry of Education, Culture, Sports, Science and Technology (No. 26430043; to TO).*
How to cite this article: *Sugeno A, Piao W, Yamazaki M, Takahashi K, Arikawa K, Matsunaga H, Hosokawa M, Tominaga D, Goshima Y, Takeyama H, Ohshima T (2021) Cortical transcriptome analysis after spinal cord injury reveals the regenerative mechanism of central nervous system in CRMP2 knock-in mice. Neural Regen Res 16(7):1258-1265.*

with intrinsic factors is yet to be revealed.

Collapsin response mediator protein 2 (CRMP2) is one such candidate protein which is abundantly expressed in the adult mammalian brain (Wang and Strittmatter, 1996). CRMP2 is a member of the CRMP family proteins (CRMP1-5) which were identified as downstream molecules from Semaphorin 3A - an axon guidance cue (Schmidt and Strittmatter, 2007). CRMP2 has been reported to bind to microtubules, kinesin or dynein dependent vesicles, transport proteins, and interact with calcium channels (Kawano et al., 2005; Kimura et al., 2005; Wang et al., 2009; Rahajeng et al., 2010; Lin et al., 2011). Through these complex interactions, CRMP2 regulates synaptic transmission (Brittain et al., 2009; Wang et al., 2009), controls microtubule dynamics (Zheng et al., 2018), and modulates vesicle trafficking (Arimura et al., 2009; Rahajeng et al., 2010). The activity of CRMP2 is controlled by phosphorylation and Cdk5 is one of the major upstream kinases that phosphorylates CRMP2 at Ser522. Recently, in a mouse model, inhibition of phosphorylation at Ser522 (CRMP2KI) induces axon elongation after SCI along with reduced inflammation and microtubule stabilization at the spinal cord lesion site (Nagai et al., 2016). CRMP2KI mice showed partial recovery in the lost sensorimotor function subsequently and the phosphorylation inhibition of CRMP2 at Ser522 was suggested to have a therapeutic effect on SCI pathophysiology (Nagai et al., 2016).

The pathophysiology of SCI was also observed in the brain sensorimotor cortex. The axotomized neurons and neighborhood neurons significantly shrink and the number of synaptic spines reduces after SCI (Barron et al., 1988; Kim et al., 2006; Carter et al., 2008; Ghosh et al., 2012). These structural change is known to contribute to the rewiring of neuronal circuits within the cortex for compensating the lost sensorimotor functions (Ghosh et al., 2010). The effect of such changes in the cortex on the entire pathophysiology of SCI is not clearly understood and it has also not been investigated in the context of CRMP2 knock-in (CRMP2KI) mouse models.

In order to clear out such cortex pathology after SCI, we analyzed the structural pathophysiology and mRNA transcription in the cortex of CRMP2KI mice.

Materials and Methods

Animals and surgical procedures

Female wild-type (WT) and CRMP2KI (Crmp2KI/KI) mice (Yamashita et al., 2012) were crossed with YFP-H (thy1-Yellow Fluorescent Protein Mouse line H) or GFP-M (thy1-Green Fluorescent Protein Mouse line M) mice (Feng et al., 2000). Offspring at the age of 6–9 weeks, weighing 22–28 g, were used in the study.The fluorescent signal was used as a landmark to demarcate the region of interest–cortex layer V. Animals were randomly selected for sham or SCI models. For the SCI model, dorsal transection at T7–8 spinal cord was performed as previously described (Hill et al., 2009; Nagai et al., 2015). In brief, mice were anesthetized by inhalation with 2–5% isoflurane (DS Pharma Animal Health, Japan) and a T7–8 laminectomy was performed with 1.5-mm-deep dorsal transection. After surgery, manual bladder evacuation was done every day. All animals could easily access food and water. SCI mice who showed 0–1 Basso Mouse Scale (BMS) score (Basso et al., 2006) at 1 day after SCI were used for the experiments. For RNA sequencing, sham-operated model was made in order for precise analysis. In the condition of sham-operated model, mice were kept under anesthesia for 15–20 min. All animals were group-housed (N = 2 to 4 per cage) in plastic cages and maintained on a 12/12-hour light/dark cycle with the room temperature (RT) maintained at 25 ± 2°C. All these experiments were performed in accordance with the guidelines of the Institutional Animal Care and Use Committee at Waseda University, Japan (2017-A027 approved on March 21, 2017; 2018-A003 approved on March 25, 2018; 2019-A026 approved on March 25, 2019).

Soma size analysis by YFP signal

Mice were anesthetized using diethyl ether (Wako, Osaka, Japan) and transcardially perfused with 4% paraformaldehyde (PFA) (nacalai tesque, Kyoto, Japan) in phosphate buffer saline (pH 7.4), one or four weeks after surgery. Brains were dissected out from the animals and post-fixed overnight. They were continuously soaked in PBS, 10% sucrose and 20% sucrose for 12–24 hours and embedded in 2:1 mixture of Tissue Tek® optimal cutting temperature (OCT) compound (Sakura Finetek Japan, Osaka, Japan) and 20% sucrose. Frozen brains were sectioned into 30 µm sections by cryostat (Leica biosystems, Wetzlar, Germany). Slices containing bregma-posterior 0.5 mm, which has been reported to be sensorimotor cortex of the hindlimbs in mice by retrograde tracer (Ghosh et al., 2012), were observed by confocal microscope (FV-1000, Olympus, Tokyo, Japan) in 1.5 µm Z-stacks. Soma size of YFP-positive neurons in the cortex layer V between 500 and 1500 µm from the midline was measured with ImageJ software ver 1.52a (NIH, Bethesda, MD, USA) (Schneider et al., 2012) by encircling the soma.

Golgi-stain and spine analysis

Female mice at the age of 6 weeks were used for spine analysis for enhanced precision. SliceGolgi Kit (Bioenno Tech, LLC, Santa Ana, CA, USA) was used for Golgi staining technique. All the procedures were performed following SliceGolgi Kit instructions except the impregnation period. In brief, dissected brains fixed in fixative solution overnight at 4°C. Hindlimb sensorimotor cortex was sliced (200 µm) by vibratome (Micro Slicer DTK-1000, D.S.K, Kyoto, Japan) and Golgi-stained with impregnation period of 2.5–3 days. Apical dendrites of pyramidal neurons in cortex layer V were selectively observed with bright-field microscope (BX51, Olympus) within 7 days after Golgi-staining. The observed dendrites were selected randomly after confirming proper staining of the dendrites as well as ensuring the dendrites did not overlap with neighboring dendrites for the ease of analysis. All the spines and spine-like protrusions on the apical dendrites were counted with 60× objective lens (UPLFLN 60X, Olympus) and the length of the dendrites was measured with ImageJ software (Schneider et al., 2012).

Immunostaining

Mice brain sections were prepared as described above. From bregma to bregma posterior 1.0 mm, the brains were sectioned into 15 µm. The slices were washed with PBS for 30 minutes, blocked with 3% horse serum in 0.1% PBSTr (PBS with 0.01% Triton X-100) for 10 minutes, 3% horse serum in 0.01% PBSTr for 30 minutes and incubated with anti-Hbα rabbit monoclonal IgG (1:50, Cat# SN70-09, Invitrogen, Carlsbad, CA, USA) overnight at 4°C. Slides were washed three times for 10 minutes each with 0.01% PBSTr the following day and incubated with Alexa Fluor 594 (1:1000, Abcam, Tokyo, Japan) rabbit IgG for 1 hour at room temperature. Following 3 times of 0.01% PBSTr washing, slices were incubated for 30 min with Hoechst 33258 (Fujifilm, Tokyo, Japan). Subsequently, the sections were washed with 0.01% PBSTr three times and mounted with Fluoromount™ aqueous mounting medium (MERCK). Images were acquired by confocal laser scanning microscope in 1.5 µm Z-stacks (FV1000, Olympus).

Tissue dissection for RNA sequencing

Female mice at the age of 6 weeks were used for enhanced precision. The mice brains were dissected out 1 week after sham or SCI operation. Mice bodies were laid on ice to prevent degradation of RNA during the dissection process. Fresh brains were temporarily stored in PBS on ice, embedded in SCEM (Super Cryoembedding Medium, SECTION-LAB Co.

Ltd., Hiroshima, Japan) using liquid nitrogen and stored at –80°C until sectioning. Fresh brains were sectioned at 30 µm thickness coronally with Cryostat (CM1860, Leica). The slices were mounted on FrameSlides PPS-Membrane 4.0 µm (Leica) and fixed immediately by air-drying. Dried-mounted slices were stored at room temperature or –20°C until use. Air-drying was conducted every time when the slices were taken out from –20°C freezer in order to prevent RNA degradation by condensation. Micro-dissection punching (Yoda et al., 2017) was performed for sampling cortex layer V, whose pyramidal neurons project axons to the spinal cord. The standard area of punching was determined by the YFP signal of YFP-H lines (Feng et al., 2000). Hindlimb sensorimotor cortex was also selected from micro-dissected samples as described previously (Ghosh et al., 2012). We confirmed the area similarly by Fast Blue tracer as well (**Additional Figure 1**).

Library construction and RNA sequencing

cDNA libraries were made after Poly (A)+ RNA extraction as per an available protocol with Smart-seq2 (Picelli et al., 2014). RNA quality was confirmed with RIN > 7 using bulk whole brain slice sample. Sequencing libraries were constructed by Nextera XT DNA library prep kit (Illumine®, San Diego, CA, USA). Constructed libraries were sequenced by paired-end way with Illumina MiSeq (Illumine®). Adapter sequences were trimmed with FLEXBAR (Dodt et al., 2012) and trimmed sequence reads were aligned to the Ensembl mouse reference genome (GRCm38 ver.92) using HISAT2 (Kim et al., 2015) with the default parameters. Annotated gene expression data was normalized as transcripts per million (TPM) value.

Differential gene expression and pathway analysis

The samples with high portion of mitochondrion genes (TPM ≥ 35%) and low number of detected genes (≤ 10,000 genes) were removed from analysis. Genes expressing more than 5 as averaged TPM value and detected in more than 4 samples from each condition (WT + sham, WT + SCI, CRMP2KI + sham, and CRMP2KI + SCI) were statistically analyzed as shown in statistics section. For pathway enrichment analysis, Gene Ontology (GO, http://www.geneontology.org), Kyoto Encyclopedia of Genes and Genomes (KEGG, http://www.genome.jp/kegg/), Reactome (https://reactome.org/), and Hallmark gene sets from MSigDB (Liberzon et al., 2015) databases from Molecular Signatures Database (MSigDB, https://www.gsea-msigdb.org/gsea/msigdb/collections.jsp) (Liberzon et al., 2011) were used with clusterProfiler (Yu et al., 2012), ReactomePA (Yu and He, 2016), and msigdbr R packages. Fold change (FC) was calculated using averaged TPM value. FC evaluation for finding differentially expressed genes (DEGs) (Top DEGs) was performed by averaging intensity-based z-score. Concretely, genes were separated into several groups by averaged TPM from sham samples and z-score was calculated from the FC values within the group. This procedure was performed repeatedly with different grouping threshold and z-scores were averaged. Genes showing the highest or the lowest averaged z-score were defined to be the top DEGs.

Quantitative real-time PCR validation

cDNA libraries for RT-qPCR validation were constructed with the same procedure as RNA sequencing library construction. SYBR Green PCR Master Mix (Applied Biosystems, Foster City, CA, USA) was used for qPCR. Reactions were carried out in triplicates with 10 ng of cDNA and 200 nM of each primer in a final volume of 20 µL. The reaction protocol was 95°C for 1 minute; 40 amplification cycles at 95°C for 15 seconds, 50°C for 30 seconds, 72°C for 1 minute. Relative quantification of gene expression was analyzed with ΔΔCt method and the internal control ACTB, whose mRNA expression did not change statistically in the RNA sequencing experiments. Genes and primers used for validation are as follows: ACTB-F (TTG TGT AAG GTA AGG TGT GC), ACTB-R (GGT TGA GGT GTT GAG GCA G), Hba-F (ATG CCC ACA AGC TGC GT), Hba-R (GTG CTC ACA GAG GCA AGG AA), Hbb-F (GCC CAG CAC AAT CAC GA), and Hbb-R (TGC CTT TAA CGA TGG CCT GA). In order to calculate relative expression ratio of Hb genes, ACTB was used as a housekeeping control for qPCR analysis.

Statistical analysis

For the comparison of soma size distribution analysis, Kolmogorov-Smirnov test was performed with GraphPad Prism software version 6.0b (GraphPad Software Inc., San Diego, CA, USA). Statistical differences of spine analysis were calculated with an unpaired two-tailed Student's *t*-test. DEGs were defined using Wilcoxon test. Adjusted *P*-values were calculated with Benjamini-Hochberg method. Genes and pathways with *P*-value < 0.05 were defined as significantly changed or enriched.

Results

CRMP2KI suppresses somatic atrophy in sensorimotor cortex after spinal cord injury

A previous study demonstrated that neurons of the corticospinal tract showed somatic atrophy after SCI in rat and mice (Barron et al., 1988; Carter et al., 2008). In mice, cortical layer V neurons undergo severe atrophy at 4 weeks after SCI (Carter et al., 2008). In order to check whether these changes occur upon the inhibition of phosphorylation of CRMP2, we examined the size of the sensorimotor neurons in cortex layer V observing YFP signal. In WT mice, sensorimotor neurons showed severe somatic atrophy at 1 week after SCI and this atrophy continued until 4 weeks after SCI (**Figure 1A** and **B**). However, in CRMP2KI mice, sensorimotor neurons shrank more mildly at 1 week after SCI and recovered to their original size at 4 weeks after SCI (**Figure 1A** and **B**). Between WT and CRMP2KI mice, significant difference was observed for both 1 week and 4 weeks after SCI ($P < 0.05$; **Figure 1C**).

CRMP2KI suppresses postsynaptic spine reduction in sensorimotor cortex after spinal cord injury

Neurons of the corticospinal tract have fewer post-synaptic spines after SCI (Ghosh et al., 2012; Kim et al., 2006). In order to reveal the effect of phosphorylation inhibition of CRMP2 on synaptic pathology, we analyzed the spine density. The location of analysis was apical dendrites of the pyramidal neurons. The number of spines decreased 1 week after SCI in WT mice (**Figure 2**). However, CRMP2KI mice did not show any changes in spine density (**Figure 2B**). CRMP2KI mice had originally fewer spines on the pyramidal neurons in cortex layer V at 7 weeks.

Cortical transcriptome profiles in all comparisons

We found the structural pathologies in sensorimotor cortex were suppressed in synaptic and somatic levels by the phosphorylation inhibition of CRMP2. However, the intracellular response in axotomized neurons is not fully understood. To reveal the detailed pathophysiology in axotomized neurons of the cortex, we performed RNA sequencing for micro-dissected cortex layer V (**Figure 3A**), 1 week after SCI in WT and CRMP2KI mice. For the precise detection of DEGs, we performed statistical analysis for each pair of groups instead of multiple comparisons. We identified 967 genes in WT mice and 811 genes in CRMP2KI mice as DEGs after SCI. The mutation effect of CRMP2 phosphorylation inhibition was analyzed using the sham model samples of WT and CRMP2KI mice. A total of 1674 DEGs were found in CRMP2KI mice compared with WT mice. PCA analysis was performed with all DEGs' TPM data and micro-dissected samples were separated well reflecting experimental conditions (**Figure 3B**). We found that the number of overlapped DEGs did not account for the high percentage of whole DEGs (**Figure 3C**).

Differential gene expression by the phosphorylation inhibition of CRMP2

We analyzed the mutation effect of CRMP2 phosphorylation inhibition. We detected 1674 DEGs. Among them, 1176 genes were upregulated, while 498 genes were downregulated (**Additional Figure 2**). Pathway enrichment analysis revealed that many pathways related to intracellular metabolism and neuronal functions were differentially expressed in CRMP2KI sensorimotor cortex (**Table 1** and **Additional Table 1** and **2**). Further, genes involved in the cytosolic or mitochondrial translation and oxidative phosphorylation, proteasome, spliceosome pathways were significantly upregulated ($P < 0.05$, $q < 0.05$), and fatty acid metabolism, lysosome, neuronal system, synaptic pathway genes were downregulated ($P < 0.05$, $q < 0.2$). In addition to the oxidative phosphorylation and ribosomal pathways in mitochondria, genes regulating mitochondrion organization were also upregulated (**Additional Figure 2C**). GO analysis also displayed that neuronal specific structural or functional terms such as axon, and vesicles were enriched among downregulated DEGs (**Additional Figure 2D**). This suggests that the inhibition of phosphorylation of CRMP2 might dynamically change the intracellular metabolic system and neuronal functions. We also analyzed the top 20 significant DEGs (**Additional Tables 3** and **4**). Various genes whose function is restricted to cytoskeletal protein binding like Nrcam, Map1b, and Vapa were greatly downregulated.

Table 1 | Enriched biological pathways of differentially expressed genes after SCI in WT and CRMP2KI mice

	Up-regulation	Down-regulation
CRMP2KI *vs*. WT	Translation	Fatty acid metabolism
	Oxidative phosphorylation	Lysosome
	Metabolism of RNA	Neuronal system
	Proteasome	Neutrophil degranulation
	DNA repair	Transport of small molecules
	Spliceosome	Transmission across chemical synapses
WT: SCI *vs*. sham	Translation	
	Oxidative phosphorylation	
CRMP2KI: SCI *vs*. sham	Channel activity	Neuronal system
		Transmission across chemical synapses
		Translation
		Glial cell differentiation
		Myelin sheath
		Synaptic vesicles

CRMP2: Collapsin response mediator protein 2; KI: knock-in; SCI: spinal cord injury; WT: wild-type.

Differential gene expression after spinal cord injury in WT and CRMP2KI mice

We detected 967 DEGs after SCI in WT mice. Of them, 886 DEGs showed upregulation. Pathway analysis revealed that cytosolic or mitochondrial translation and oxidative phosphorylation pathway genes were significantly enriched among the upregulated genes (**Table 1** and **Additional table 5**). From the limited number of 81 downregulated genes, we could not detect any enriched pathways. Interestingly, hemoglobin genes Hba-a1, Hba-a2, Hbb-bs, and Hbb-bt were remarkably upregulated and became the top 4 upregulated genes (FC > 6.9) after SCI (**Table 2**).

On the other hand, in CRMP2KI mice, we detected a total of 811 DEGs in which 224 were upregulated; while 587 were downregulated after SCI (**Additional Figure 3**). Upregulated cluster consisted mainly of channel and transporter activity genes (**Table 1** and **Additional figure 3C**). From the downregulated genes, neuronal system and cytosolic translation pathway genes were specifically enriched. Genes regulating synaptic activity and organization of axon, myelin sheath, vesicles, and synaptic membranes were all downregulated (**Figure 4A** and **Additional Table 6**). Notably, gliogenesis, glial cell differentiation, and developmental genes were also enriched in the downregulated DEGs after SCI in CRMP2KI mice (**Additional Table 6**). Hemoglobin genes were not differentially expressed in CRMP2KI mice because of the broad distribution of TPM values.

As summarized in **Table 1**, oxidative phosphorylation pathway genes were upregulated in both CRMP2KI mutation and SCI. In order to compare these DEGs expression level in other condition, heatmap was generated for DEGs after SCI in WT mice and pathway analysis was performed for several clusters (**Figure 4B**). We found that oxidative phosphorylation pathway and mitochondrial component genes were expressed at a high level in both CRMP2KI + sham and CRMP2KI + SCI condition compared with WT + SCI condition.

Hemoglobin expression in sensorimotor cortex after SCI

In transcriptome analysis, four hemoglobin genes were remarkably upregulated after spinal cord injury in WT mice (**Table 2**). These hemoglobin expressions were validated with RT-qPCR at first. cDNA libraries were prepared from micro-dissected sensorimotor cortex. Both Hba and Hbb genes were significantly upregulated after SCI in WT mice (**Figure 5A**). However, there was no significant difference between sham and SCI in CRMP2KI mice. These results were consistent with the transcriptome analysis obtained from RNA sequencing.

Next, we performed immunostaining of Hbα in WT mice to analyze if this hemoglobin upregulation could occur at the protein level in the sensorimotor cortex after SCI. The ratio of Hbα positive cells increased after SCI but not significantly ($P = 0.063$) unlike our expectation (**Figure 5B**).

Discussion

The inhibition of CRMP2 phosphorylation has been proven to be effective for the diagnosis of SCI by this study. Previous study showed that the phosphorylation inhibition of CRMP2 suppresses glial scar formation and inflammation at the spinal cord lesion, which leads to axonal regeneration (Nagai et al., 2016). In this study, we found that spine reduction and somatic atrophy were suppressed in the sensorimotor cortex in CRMP2KI mice. Spine reduction is considered to regulate the rewiring of neuronal circuits as compensation for lost sensorimotor function and brain activity map changed in rat SCI model (Ghosh et al., 2010, 2012; Zhang et al., 2015). We show that CRMP2KI mice have the same spine density as the originally fewer density, 1 week after SCI. According to the previous study (Jin et al., 2016), fewer spines were also observed in CA1 pyramidal neurons of CRMP2KI mice at the age of 5 weeks. Focusing on the effect of SCI, the phosphorylation inhibition of CRMP2 suppressed further spine reduction by SCI. Although it is necessary to take into account that there might be relevance between suppression of spine reduction after SCI and the original fewer spines in CRMP2KI mice, the phosphorylation inhibition of CRMP2 suppressed further post-synaptic spine reduction by SCI from the primary number. This supports the idea that it could be possible in CRMP2KI mice, there is only a mild alteration of electrical activity in the somatosensory cortex, with concomitant suppression of somatic atrophy and spine reduction. Simultaneously, somatic atrophy gave an indication of neuronal stress after SCI. Significant somatic atrophy is observed 4 weeks after SCI in WT mice, but somatic size in CRMP2KI regained the original size on the same time scale. This result suggests that phosphorylation inhibition of CRMP2 contribute to suppressing the somatic atrophy of axotomized neurons and facilitating the recovery toward original size after SCI. This size recovery is also observed in the mice treated with ChABC which have retrograde neuroprotective effect

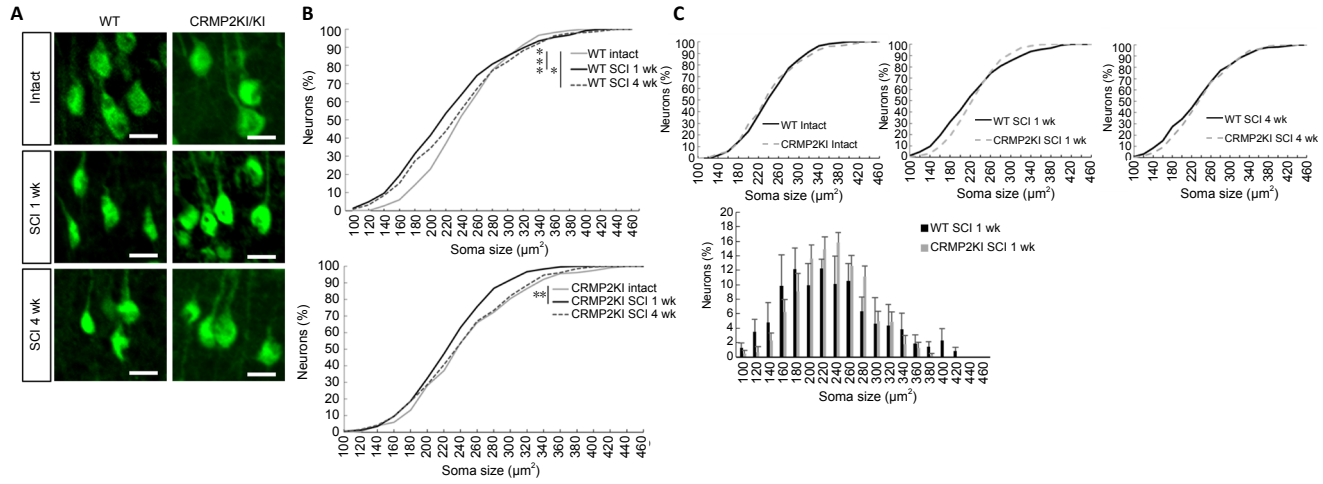

Figure 1 | **Constitutively activated CRMP2 suppresses soma atrophy in corticospinal neurons after SCI.**
(A) YFP-labeled Layer V neurons (green) show severe atrophy 1 week after SCI and partially recovered 3 weeks later. *N* = 3, 4, 3, 3, 4, 3 for wild-type (WT), WT + SCI 1 wk, WT + SCI 4 wk, CRMP2KI, CRMP2KI + SCI 1 wk, CRMP2KI + SCI 4 wk, respectively. Scale bars: 20 μm. (B) Distribution of soma size of YFP-labeled layer V after SCI in WT (above) and CRMP2KI (below) mice (Kolmogorov-Smirnov test, **P* < 0.05, ***P* < 0.01, ****P* < 0.001). (C) Distributions of soma size were compared between WT and CRMP2KI mice at 1 and 4 weeks after injury. CRMP2: Collapsin response mediator protein 2; KI: knock-in; SCI: spinal cord injury.

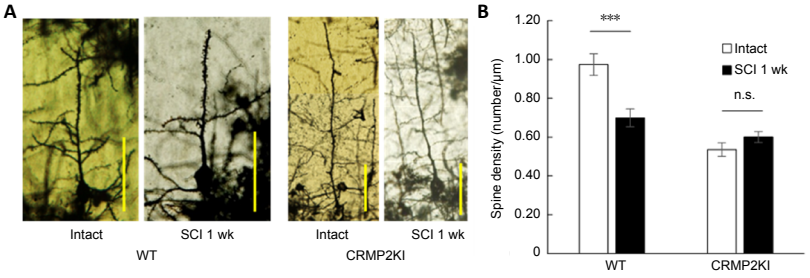

Figure 2 | **Constitutively activated CRMP2 suppresses spine decrease in CST neurons after SCI.**
(A) Golgi-stained layer V neurons after SCI in WT and CRMP2 KI mice. Scale bars: 50 μm. (B) Spine density of layer V neurons was calculated from apical dendrites (*n* = 17, 25, 25, 30 for WT, WT + SCI 1 wk, CRMP2KI, CRMP2KI + SCI 1 wk, respectively). Data are presented as the mean ± SEM. ****P* < 0.001 (Student's *t*-test). CRMP2: Collapsin response mediator protein 2; KI: knock-in; SCI: spinal cord injury; WT: wild-type.

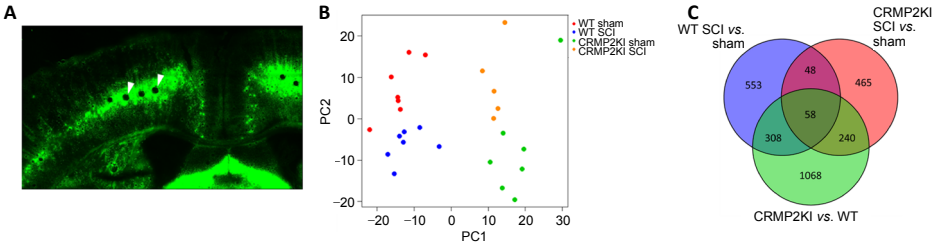

Figure 3 | **RNA sequencing analysis of micro-dissected samples.**
RNA sequencing analysis was performed for micro-dissected samples obtained from the hindlimb sensorimotor cortex layer V. Each condition has 5–7 micro-dissected samples from 3, 4 mice. (A) Mouse cortex slice of bregma posterior 0.5 mm. YFP fluorescence was used to mark the dissection regions. Arrows indicate the micro-dissected regions of 100 μm diameter. (B) Principal component analysis (PCA) of micro-dissected samples. Transcripts per million (TPM) data of all differentially expressed genes (DEGs) found in three comparisons, i.e., SCI *vs*. sham in wild-type (WT), SCI *vs*. sham in CRMP2KI, CRMP2KI sham *vs*. WT sham, were used. (C) The number of overlapped DEGs found in three comparisons was shown in Venn diagram. CRMP2: Collapsin response mediator protein 2; KI: knock-in; SCI: spinal cord injury.

Table 2 | **Top 10 significantly upregulated DEGs after spinal cord injury in WT mice**

Rank	Genes	Sham average TPM	SCI average TPM	*P*-value	Fold change	Average z-score	2KI SCI *vs*. sham	2KI *vs*. WT
1	Hbb-bt	28.9	253.19	0.02	8.76	29.91	FC 1.40	FC 10.31
2	Hba-a1	73.39	538.72	0.01	7.34	20.18	FC 1.75	FC 5.81
3	Hba-a2	84.98	623.03	0.01	7.33	20.15	FC 1.93	FC 5.62
4	Hbb-bs	85.31	593.45	0.04	6.96	18.94	FC 1.50	FC 7.41
5	Cort	11.42	34.11	0.001	2.99	7.32	FC 1.46	FC 1.30
6	Yjefn3	12.78	37.79	0.02	2.96	7.21	–	–
7	Pygm	11.53	31.13	0.001	2.7	6.2	FC 1.10	FC 1.08
8	Gm47441	26.52	69.31	0.002	2.61	5.91	FC 0.64	↑FC 4.19
9	Gm10591	12.44	32.2	0.004	2.59	5.78	FC 0.86	FC 1.45
10	Gm23935	9.76	26.77	0.05	2.74	5.65	FC 0.54	FC 2.54

Arrow (↑) indicates DEGs between comparison. DEGs: Differentially expressed genes; 2KI: collapsin response mediator protein 2 knock-in; SCI: spinal cord injury; TPM: transcripts per million; WT: wild-type.

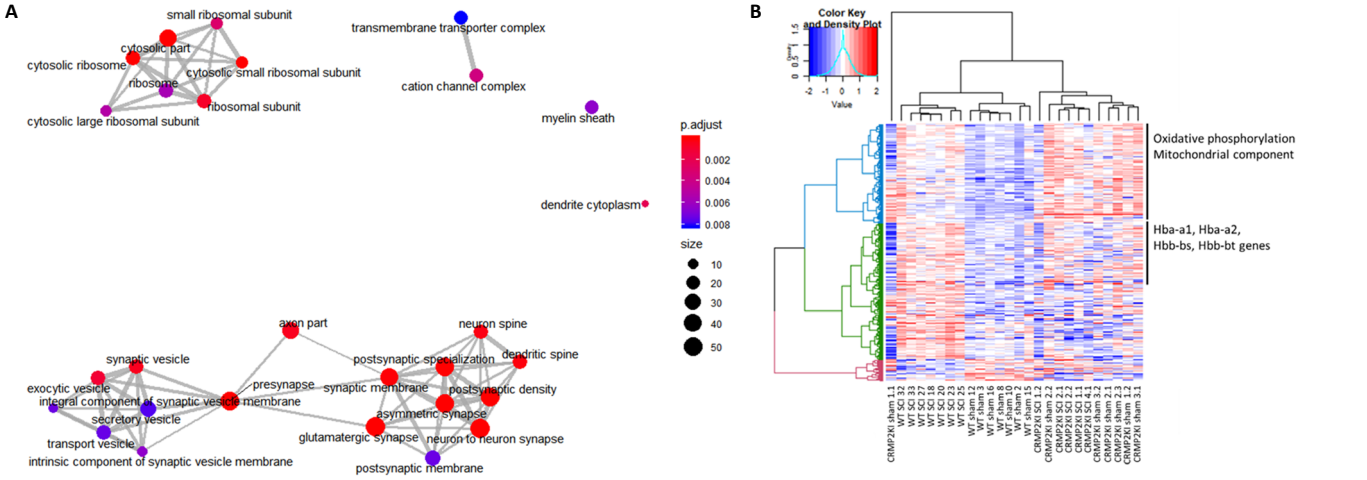

Figure 4 | **Differential gene expression analysis after SCI.**
(A) Cellular component GO enrichment analysis of downregulated genes after SCI in CRMP2KI mice. Many neuronal specific genes were enriched in addition to ribosomal pathway genes. P. adust: Adjusted P-value calculated with Benjamini-Hochberg method. (B) Heatmap using the differentially expressed genes (DEGs) after SCI in wild-type (WT) mice. The clusters containing characteristic enriched pathways and hemoglobin genes have been shown alongside. (n = 5–7, N = 3,4). CRMP2: Collapsin response mediator protein 2; KI: knock-in; SCI: spinal cord injury.

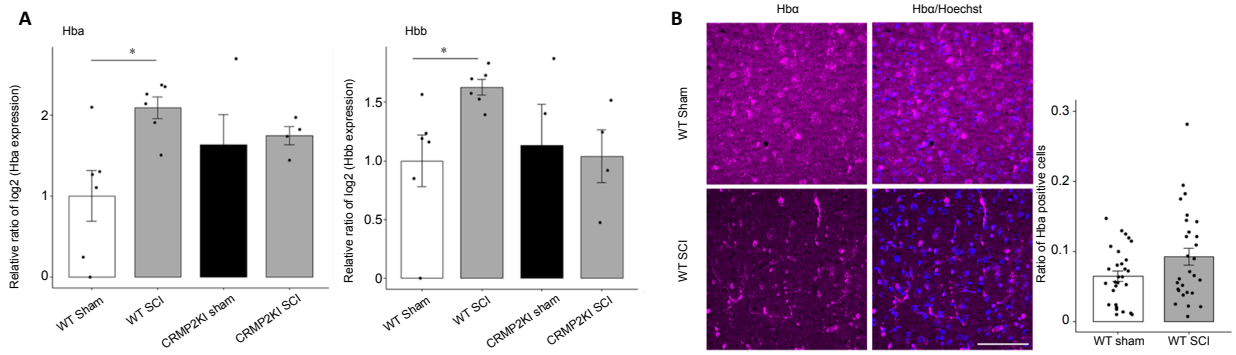

Figure 5 | **Hemoglobin (Hb) was upregulated after SCI and increased at protein level.**
(A) mRNA levels of Hba and Hbb were validated by RT-qPCR from the micro-dissected samples 1 week after SCI (n = 6, 6, 4, 4 for wild-type (WT) sham, WT SCI, CRMP2KI sham, CRMP2KI SCI, respectively). *P < 0.05 (Student's t-test). (B) Immunostaining of Hbα in hindlimb sensorimotor cortex in WT mice. The ratio of Hbα positive cells was analyzed with respect to Hoechst staining (3–7 micro-dissected samples were obtained from five mice). Scale bars: 100 µm. Data are presented as the mean ± SEM. CRMP2: Collapsin response mediator protein 2; KI: knock-in; SCI: spinal cord injury.

after SCI (Carter et al., 2008). This gave us the possibility that the phosphorylation inhibition of CRMP2 also have similar neuroprotective effect in axotomized neurons. Considering the sensorimotor structural pathology after SCI, the phosphorylation inhibition of CRMP2 contributes to suppressing SCI pathology not only at the spinal cord lesion site; but also in the intracellular response of CNS neurons.

We also performed RNA sequencing analysis in micro-dissected sensorimotor cortex to reveal the detailed intracellular response in axotomized neurons after SCI in WT and CRMP2KI mice. Each cortical transcriptome profile has different characteristics when subjected to SCI, CRMP2 mutation and both. We observed that genes involved in the cytosolic, mitochondrial translation and oxidative phosphorylation pathways were significantly upregulated after SCI. Previous studies showed that genes involved in similar pathways like translation, RNA splicing, and oxidative phosphorylation were differentially expressed within a week after SCI in the cortex (Jaerve et al., 2012; Baek et al., 2017). This showed that our transcriptome analysis with micro-dissected cortex is consistent with the previous studies. One of these studies also suggested that impaired oxidative phosphorylation and mitochondrial dysfunction occur after SCI (Baek et al., 2017). We also found upregulation of mitochondrion component genes. Oxidative phosphorylation pathway takes place in mitochondria and impaired oxidative phosphorylation induces oxidative stress by generating reactive oxygen species (ROS) in cells generally. ROS and oxidative stress have been considered to be a hallmark of SCI and progressive SCI pathology at spinal cord lesion sites (Xu et al., 2005; Jia et al., 2012). In addition, one transcriptome analysis in cortex layer V also detected differential expression in response to oxidative stress (Kruse et al., 2011). Our findings regarding upregulated genes and enriched pathways after SCI in WT also suggests the oxidative stress as well. Notably, we further detected 4 hemoglobin (Hb) genes remarkably increased after SCI in WT mice, which was also validated by qPCR. Recently, Hb was found to be expressed in CNS tissues, including cortical neurons. Also, some studies on neurodegenerative diseases such as Alzheimer's disease, Multiple Sclerosis, and Parkinson's disease suggested the relevance between Hb and their pathophysiology (Biagioli et al., 2009; Richter et al., 2009; Schelshorn et al., 2009; Brown et al., 2016; Freed and Chakrabarti, 2016; Altinoz et al., 2019). In the field of SCI studies, this is the first report that indicates the involvement of Hb in SCI pathophysiology. The role of Hb in nervous system has not been fully understood and continuous studies were needed for clear explanation. However Hb is suggested to be involved in O_2 homeostasis and mitochondrial homeostasis by buffering protons by other studies (Biagioli et al., 2009; Freed and Chakrabarti, 2016; Altinoz et al., 2019). Though we could not detect statistically significant upregulation of Hb at the protein level, Hb transcription upregulation and simultaneously upregulated

Hb functions, oxidative phosphorylation gave us some idea that the involvement of oxidative stress or impairment of mitochondrial homeostasis in axotomized neurons after SCI.

In this study, we reveal for the first time the mRNA transcription profile in sensorimotor cortex in CRMP2KI in sham-operated and SCI condition. Completely different pathways were up- or down-regulated after SCI. All the enriched pathways except the pathways involved in translation were related to typical functions of nervous system and most of the enriched pathways were downregulated after SCI. The point to be emphasized is that genes regulating synaptic compartments and functions were strongly downregulated simultaneously with the suppression of spine reduction after SCI. In addition, similar synaptic pathways were downregulated by the genetic modification of CRMP2 originally. This means axotomized neurons in CRMP2KI have quite lower mRNAs regulating synaptic functions. Although further studies are needed for clarifying the concrete mechanism, it is likely that downregulation of synaptic genes contributes to the suppression of spine reduction after SCI in CRMP2KI and might contribute to the improvement of SCI pathophysiology as well. We also found an interesting observation that glial cell differentiation and myelin sheath pathways were downregulated after SCI in CRMP2KI mice. Besides, some studies showed that microglial activation appeared in cortex (Wu et al., 2014a, b; Jure and Labombarda, 2017). We could not detect the pathway of microglial activation after SCI in WT mice, but downregulation of glial cells differentiation pathway in CRMP2KI indicates that there might be some changes in the response of glial cells including microglia, astrocytes and oligodendrocytes upon the phosphorylation inhibition of CRMP2. Indeed, the glial scar formation and inflammation at spinal cord lesion was suppressed in CRMP2KI mice (Nagai et al., 2016). Our transcriptome analysis in sensorimotor cortex indirectly supports the different response after SCI in glial cells in CRMP2KI. In addition, axon elongation was also confirmed after SCI in CRMP2KI (Nagai et al., 2016) mice. The downregulation of genes regulating myelin sheath could be involved in suppressed retrograde axon degeneration in CRMP2KI mice. To summarize, the downregulation of these pathways in CRMP2KI may be directly or indirectly involved in pathophysiology of SCI, spine reduction, glial scar formation, and axon degeneration.

It is also important that we found several metabolic intracellular pathways and synaptic compartments are differentially expressed in CRMP2KI mice. Genes involved in translation, oxidative phosphorylation and proteasome pathways were upregulated and fatty acid metabolism, lysosome pathways, and synaptic compartments were downregulated. These changes in the metabolic pathways might come from protein-protein interactions of CRMP2. Previously, CRMP2 interactome analysis indicated that CRMP2 interacts with ten proteins that regulate energy metabolism and nine proteins that regulate protein metabolism including ribosomal subunit (Martins-de-Souza et al., 2015). The interactions between these proteins and mutated CRMP2 is not clear, but the phosphorylation inhibition of CRMP2 could change these interaction levels as well and affect the metabolic system overall. Our transcriptome results are partly consistent with and partly contradict the previous proteome study interestingly. The protein levels of molecules regulating oxidative phosphorylation, proteasome and fatty acid metabolism pathways were actually decreased in CRMP2KI mice (Nakamura et al., 2018). It is possible that the phosphorylation inhibition of CRMP2 broadly induce the improvements in SCI pathophysiology via intracellular metabolic pathways. In addition, a previous phosphoproteome analysis in CRMP2KI mice indicated proteins regulating synaptic functions had different phosphorylation profile as well (Nakamura et al., 2018). Our results that genes involved in regulating synaptic compartments were differentially expressed in CRMP2KI mice might be caused by this alteration of phosphorylation in synaptic proteins. We also found that genes regulating oxidative phosphorylation and mitochondrial components were even more upregulated in both CRMP2KI condition than SCI in WT mice. It is possible that the phosphorylation inhibition of CRMP2 might already have similar condition as observed after SCI in WT mice.

In conclusion, our study showed many possibilities of SCI pathophysiology in axotomized neurons in WT and CRMP2KI mice. Further, the transcriptome profile of CRMP2KI was revealed in detail. We confirmed that CRMP2KI suppressed the structural pathophysiology of spine reduction and somatic atrophy after SCI in cortex. In addition, translation and oxidative phosphorylation pathways were upregulated in cortex after SCI. Interestingly, fatty acid metabolism, lysosome, and neuronal system relating pathways were downregulated originally by phosphorylation inhibition of CRMP2 though translation, oxidative phosphorylation, and proteasome pathways were increased. After SCI in this CRMP2 mutation, neuronal system, synaptic, translation, glial cell differentiation, and myelin sheath pathways were decreased though only channel activity function was upregulated. This transcriptome analysis indicated (1) CRMP2KI seems to influence the whole metabolic system in CNS such as oxidative phosphorylation, fatty acid metabolism, and proteasome pathways, (2) these metabolic systems might contribute to the SCI pathophysiology in axotomized neurons as well and (3) response to SCI in CRMP2KI mice seems to involve synaptic activity and glial cell differentiation in addition to the putatively effective pathways such as microtubules stabilization. Hb involvement in SCI pathology is also suggested for the first time in this study. However in this study we could not cut in the functional level. In spite of the suggestions from mRNA transcriptome, locations that each protein works and protein interaction after SCI are not directly revealed. Cell-to-cell interaction in cortex is also unclear. At this point, our methods have some limitations.

The intracellular mechanisms underlying for axon elongation and functional recovery in CRMP2KI or Hb functions in axotomized neurons are still unclear in detail. In order to clarify the concrete mechanism on CNS regeneration, the complicated SCI pathophysiology and pathophysiological phenomena in CRMP2KI need to be further investigated.

Acknowledgments: *We thank Sachiyo Aburatani, Hisashi Anbutsu and Yoriko Uotani for support in OIL, and support by the Platform Project for Supporting Drug Discovery and Life Science Research (Basis for Supporting Innovative Drug Discovery and Life Science Research (BINDS)) from AMED under Grant Number JP20am0101104.*
Author contributions: *AS, WP, MY, and KT performed experiments. AS, DT, HM, KA, and MH analyzed RNA sequencing data. TO and YG developed CRMP2KI mice. HT and TO supervised the overall project. AS and TO wrote the manuscript.*
Conflicts of interest: *The authors declare no conflict of interest.*
Financial support: *This work was supported by Grants-in-Aid for Scientific Research on Priority Areas from The Ministry of Education, Culture, Sports, Science and Technology (No. 26430043; to T.O)*
Institutional review board statement: *All these experiments were performed in accordance with the guidelines of the Institutional Animal Care and Use Committee at Waseda University, Japan (2017-A027 approved on March 21, 2017; 2018-A003 approved on March 25, 2018; 2019-A026 approved on March 25, 2019).*

Data sharing statement: *Datasets analyzed during the current study are available from the corresponding author on reasonable request.*
Plagiarism check: *Checked twice by iThenticate.*
Peer review: *Externally peer reviewed.*

credit is given and the new creations are licensed under the identical terms.

Additional files:

Additional Figure 1: *Fast blue tracer positive region of sensorimotor cortex.*

Additional Figure 2: *Transcriptome analysis between WT and CRMP2KI mice.*

Additional Figure 3: *Transcriptome analysis after spinal cord injury in CRMP2KI.*

Additional Table 1: *Enriched pathways of upregulated DEGs by the phosphorylation deficient of CRMP2 (P < 0.05, q < 0.05).*

Additional Table 2: *Enriched pathways of downregulated DEGs by the phosphorylation deficient of CRMP2 (P < 0.05, q < 0.2).*

Additional Table 3: *Top20 significantly upregulated DEGs by the phosphorylation deficient of CRMP2.*

Additional Table 4: *Top20 significantly downregulated DEGs by the phosphorylation deficient of CRMP2.*

Additional Table 5: *Enriched pathways of upregulated DEGs after spinal cord injury in WT mice (P < 0.05, q < 0.05).*

Additional Table 6: *Enriched pathways of downregulated DEGs after spinal cord injury in CRMP2KI mice (P < 0.05, q < 0.05).*

References

Altinoz MA, Guloksuz S, Schmidt-Kastner R, Kenis G, Ince B, Rutten BPF (2019) Involvement of hemoglobins in the pathophysiology of Alzheimer's disease. Exp Gerontol 126:110680.

Arimura N, Kimura T, Nakamuta S, Taya S, Funahashi Y, Hattori A, Shimada A, Ménager C, Kawabata S, Fujii K, Iwamatsu A, Segal RA, Fukuda M, Kaibuchi K (2009) Anterograde transport of TrkB in axons is mediated by direct interaction with Slp1 and Rab27. Dev Cell 16:675-686.

Baek A, Cho SR, Kim SH (2017) Elucidation of gene expression patterns in the brain after spinal cord injury. Cell Transplant 26:1286-1300.

Barron KD, Dentiger MP, Popp AJ, Makes R (1988) Neurons of layer Vb of rat sensorimotor cortex atrophy but do not die after thoracic cord transection. J Neuropathol Exp Neurol 47:62-74.

Basso DM, Fisher LC, Anderson AJ, Jakeman LB, McTigue DM, Popovich PG (2006) Basso Mouse Scale for locomotion detects differences in recovery after spinal cord injury in five common mouse strains. J Neurotrauma 23:635-659.

Biagioli M, Pinto M, Cesselli D, Zaninello M, Lazarevic D, Roncaglia P, Simone R, Vlachouli C, Plessy C, Bertin N, Beltrami A, Kobayashi K, Gallo V, Santoro C, Ferrer I, Rivella S, Beltrami CA, Carninci P, Raviola E, Gustincich S (2009) Unexpected expression of alpha- and beta-globin in mesencephalic dopaminergic neurons and glial cells. Proc Natl Acad Sci U S A 106:15454-15459.

Brittain JM, Piekarz AD, Wang Y, Kondo T, Cummins TR, Khanna R (2009) An atypical role for collapsin response mediator protein 2 (CRMP-2) in neurotransmitter release via interaction with presynaptic voltage-gated calcium channels. J Biol Chem 284:31375-31390.

Brown N, Alkhayer K, Clements R, Singhal N, Gregory R, Azzam S, Li S, Freeman E, McDonough J (2016) Neuronal hemoglobin expression and its relevance to multiple sclerosis neuropathology. J Mol Neurosci 59:1-17.

Carter LM, Starkey ML, Akrimi SF, Davies M, McMahon SB, Bradbury EJ (2008) The Yellow Fluorescent Protein (YFP-H) mouse reveals neuroprotection as a novel mechanism underlying chondroitinase ABC-mediated repair after spinal cord injury. J Neurosci 28:14107-14120.

Dodt M, Roehr JT, Ahmed R, Dieterich C (2012) FLEXBAR-flexible barcode and adapter processing for next-generation sequencing platforms. Biology (Basel) 1:895-905.

Feng G, Mellor RH, Bernstein M, Keller-Peck C, Nguyen QT, Wallace M, Nerbonne JM, Lichtman JW, Sanes JR (2000) Imaging neuronal subsets in transgenic mice expressing multiple spectral variants of GFP. Neuron 28:41-51.

Freed J, Chakrabarti L (2016) Defining a role for hemoglobin in Parkinson's disease. NPJ Parkinsons Dis 2:16021.

Ghosh A, Haiss F, Sydekum E, Schneider R, Gullo M, Wyss MT, Mueggler T, Baltes C, Rudin M, Weber B, Schwab ME (2010) Rewiring of hindlimb corticospinal neurons after spinal cord injury. Nat Neurosci 13:97-104.

Ghosh A, Peduzzi S, Snyder M, Schneider R, Starkey M, Schwab ME (2012) Heterogeneous spine loss in layer 5 cortical neurons after spinal cord injury. Cereb Cortex 22:1309-1317.

Hill RL, Zhang YP, Burke DA, DeVries WH, Zhang Y, Magnuson DSK, Whittemore SR, Shields CB (2009) Anatomical and functional outcomes following a precise, graded, dorsal laceration spinal cord injury in C57BL/6 Mice. J Neurotrauma 26:1.

Jaerve A, Kruse F, Malik K, Hartung HP, Müller HW (2012) Age-dependent modulation of cortical transcriptomes in spinal cord injury and repair. PLoS One 7:49812.

Jia Z, Zhu H, Li J, Wang X, Misra H, Li Y (2012) Oxidative stress in spinal cord injury and antioxidant-based intervention. Spinal Cord 50:264-274.

Jin X, Sasamoto K, Nagai J, Yamazaki Y, Saito K, Goshima Y, Inoue T, Ohshima T (2016) Phosphorylation of CRMP2 by Cdk5 regulates dendritic spine development of cortical neuron in the mouse hippocampus. Neural Plast 2016:6790743.

Jure I, Labombarda F (2017) Spinal cord injury drives chronic brain changes. Neural Regen Res 12:1044-1047.

Kawano Y, Yoshimura T, Tsuboi D, Kawabata S, Kaneko-Kawano T, Shirataki H, Takenawa T, Kaibuchi K (2005) CRMP-2 is involved in kinesin-1-dependent transport of the Sra-1/WAVE1 complex and axon formation. Mol Cell Biol 25:9920-9935.

Kim BG, Dai HN, McAtee M, Vicini S, Bregman BS (2006) Remodeling of synaptic structures in the motor cortex following spinal cord injury. Exp Neurol 198:401-415.

Kim D, Langmead B, Salzberg SL (2015) HISAT: A fast spliced aligner with low memory requirements. Nat Methods 12:357-360.

Kimura T, Arimura N, Fukata Y, Watanabe H, Iwamatsu A, Kaibuchi K (2005) Tubulin and CRMP-2 complex is transported via Kinesin-1. J Neurochem 93:1371-1382.

Kruse F, Bosse F, Vogelaar CF, Brazda N, Küry P, Gasis M, Müller H (2011) Cortical gene expression in spinal cord injury and repair: insight into the functional complexity of the neural regeneration program. Front Mol Neurosci 4:26.

Liberzon A, Birger C, Thorvaldsdóttir H, Ghandi M, Mesirov JP, Tamayo P (2015) The molecular signatures database hallmark gene set collection. Cell Syst 1:417-425.

Liberzon A, Subramanian A, Pinchback R, Thorvaldsdóttir H, Tamayo P, Mesirov JP (2011) Molecular signatures database (MSigDB) 3.0. Bioinformatics 27:1739-1740.

Lin PC, Chan PM, Hall C, Manser E (2011) Collapsin response mediator proteins (CRMPs) are a new class of microtubule-associated protein (MAP) that selectively interacts with assembled microtubules via a taxol-sensitive binding interaction. J Biol Chem 286:41466-41478.

Martins-de-Souza D, Cassoli JS, Nascimento JM, Hensley K, Guest PC, Pinzon-Velasco AM, Turck CW (2015) The protein interactome of collapsin response mediator protein-2 (CRMP2/DPYSL2) reveals novel partner proteins in brain tissue. Proteomics Clin Appl 9(9-10):817-831.

Nagai J, Kitamura Y, Owada K, Yamashita N, Takei K, Goshima Y, Ohshima T (2015) Crmp4 deletion promotes recovery from spinal cord injury by neuroprotection and limited scar formation. Sci Rep 5:8269.

Nagai J, Owada K, Kitamura Y, Goshima Y, Ohshima T (2016) Inhibition of CRMP2 phosphorylation repairs CNS by regulating neurotrophic and inhibitory responses. Exp Neurol 277:283-295.

Nakamura H, Takahashi-Jitsuki A, Makihara H, Asano T, Kimura Y, Nakabayashi J, Yamashita N, Kawamoto Y, Nakamura F, Ohshima T, Hirano H, Tanaka F, Goshima Y (2018) Proteome and behavioral alterations in phosphorylation-deficient mutant collapsin response mediator protein 2 knock-in mice. Neurochem Int 119:207-217.

Nakamura M, Okano H (2013) Cell transplantation therapies for spinal cord injury focusing on induced pluripotent stem cells. Cell Res 23:70-80.

Picelli S, Faridani OR, Björklund ÅK, Winberg G, Sagasser S, Sandberg R (2014) Full-length RNA-seq from single cells using Smart-seq2. Nat Protoc 9:171-181.

Rahajeng J, Giridharan SSP, Naslavsky N, Caplan S (2010) Collapsin response mediator protein-2 (Crmp2) regulates trafficking by linking endocytic regulatory proteins to dynein motors. J Biol Chem 285:31918-31922.

Richter F, Meurers BH, Zhu C, Medvedeva VP, Chesselet MF (2009) Neurons express hemoglobin α- and β-chains in rat and human brains. J Comp Neurol 515:538-547.

Schelshorn DW, Schneider A, Kuschinsky W, Weber D, Krüger C, Dittgen T, Bürgers HF, Sabouri F, Gassler N, Bach A, Maurer MH (2009) Expression of hemoglobin in rodent neurons. J Cereb Blood Flow Metab 29:585-595.

Schmidt EF, Strittmatter SM (2007) The CRMP family of proteins and their role in Sema3A signaling. Adv Exp Med Biol 600:1-11.

Schneider CA, Rasband WS, Eliceiri KW (2012) NIH Image to ImageJ: 25 years of image analysis. Nat Methods 9:671-675.

Wang LH, Strittmatter SM (1996) A family of rat CRMP genes is differentially expressed in the nervous system. J Neurosci 16:6197-6207.

Wang Y, Brittain JM, Wilson SM, Khanna R (2009) Emerging roles of collapsin response mediator proteins (CRMPs) as regulators of voltage-gated calcium channels and synaptic transmission. Commun Integr Biol 3:172-175.

Wu J, Stoica BA, Luo T, Sabirzhanov B, Zhao Z, Guanciale K, Nayar SK, Foss CA, Pomper MG, Faden AI (2014a) Isolated spinal cord contusion in rats induces chronic brain neuroinflammation, neurodegeneration, and cognitive impairment. Involvement of cell cycle activation. Cell Cycle 13:2446-2458.

Wu J, Zhao Z, Sabirzhanov B, Stoica BA, Kumar A, Luo T, Skovira J, Faden AI (2014b) Spinal cord injury causes brain inflammation associated with cognitive and affective changes: Role of cell cycle pathways. J Neurosci 34:10989-11006.

Xu W, Chi L, Xu R, Ke Y, Luo C, Cai J, Qiu M, Gozal D, Liu R (2005) Increased production of reactive oxygen species contributes to motor neuron death in a compression mouse model of spinal cord injury. Spinal Cord 43:204-213.

Yamashita N, Ohshima T, Nakamura F, Kolattukudy P, Honnorat J, Mikoshiba K, Goshima Y (2012) Phosphorylation of CRMP2 (collapsin response mediator protein 2) is involved in proper dendritic field organization. J Neurosci 32:1360-1365.

Yoda T, Hosokawa M, Takahashi K, Sakanashi C, Takeyama H, Kambara H (2017) Site-specific gene expression analysis using an automated tissue micro-dissection punching system. Sci Rep 7:4325.

Yu G, He QY (2016) ReactomePA: An R/Bioconductor package for reactome pathway analysis and visualization. Mol Biosyst 12:477-479.

Yu G, Wang LG, Han Y, He QY (2012) clusterProfiler: an R package for comparing biological themes among gene clusters. Omi A J Integr Biol 16:284-287.

Zhang K, Zhang J, Zhou Y, Chen C, Li W, Ma L, Zhang L, Zhao J, Gan W, Zhang L, Tang P (2015) Remodeling the dendritic spines in the hindlimb representation of the sensory cortex after spinal cord hemisection in mice. PLoS One 10:1-16.

Zheng Y, Sethi R, Mangala LS, Taylor C, Goldsmith J, Wang M, Masuda K, Karaminejadranjbar M, Mannion D, Miranda F, Herrero-Gonzalez S, Hellner K, Chen F, Alsaadi A, Albukhari A, Fotso DC, Yau C, Jiang D, Pradeep S, Rodriguez-Aguayo C, et al. (2018) Tuning microtubule dynamics to enhance cancer therapy by modulating FER-mediated CRMP2 phosphorylation. Nat Commun 9:476.

C-Editors: Zhao M, Li CH; T-Editor: Jia Y

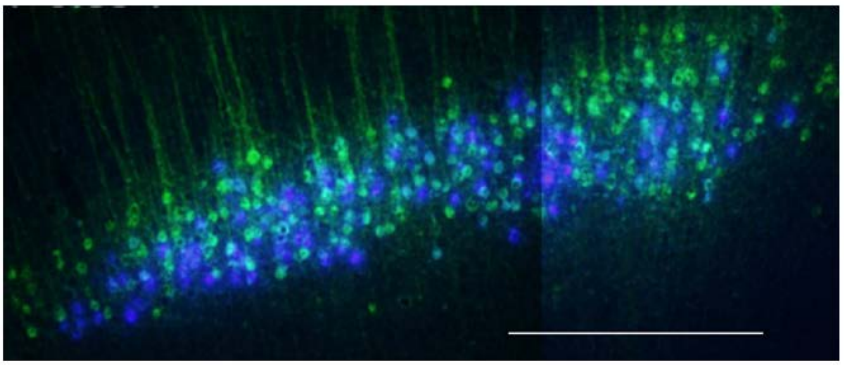

Additional Figure 1 Fast blue tracer positive region of sensorimotor cortex.

In order to clearly identify the corticospinal tract neurons whose axons were injured by spinal cord injury, fast blue (FB) tracer (blue) was injected into the spinal cord. The figure shows the overlap of YFP^+ (green) scortex layer Vneurons and FB^+ neurons. Scale bar: 400 μm.

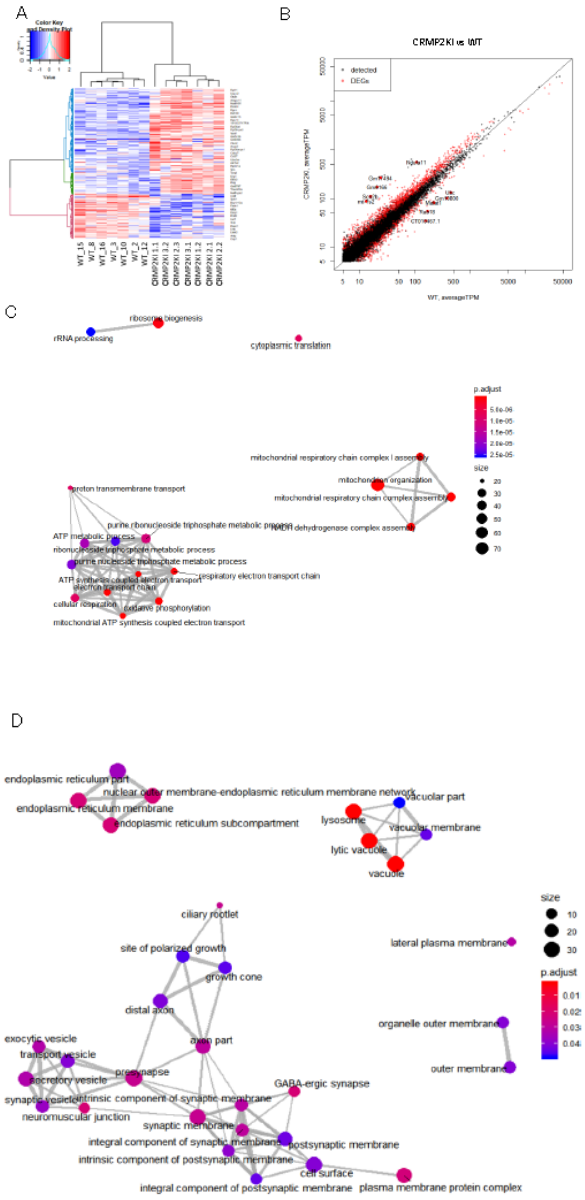

Additional Figure 2 Transcriptome analysis between WT and CRMP2KI mice.

Bioinformatic analysis of DEGs upon deficient phosphorylation of CRMP2. (A) Heatmap of all DEGs. (B) All the genes analyzed were plotted by transcripts per million values. Red represents DEGs and black represents. (B) detected genes. Gene names indicate top 5 up or down regulated genes. (C) Biological process Gene Ontology (GO) enrichment analysis of upregulated genes and (D) cellular component GO enrichment analysis of downregulated genes upon deficient phosphorylation of CRMP2. Each dot represents one GO term and the thickness of lines shows the number of shared genes between two GO terms. CRMP2: Collapsin response mediator protein 2; DEGs: differentially expressed genes; KI: knock-in; SCI: spinal cord injury; WT: wild-type.

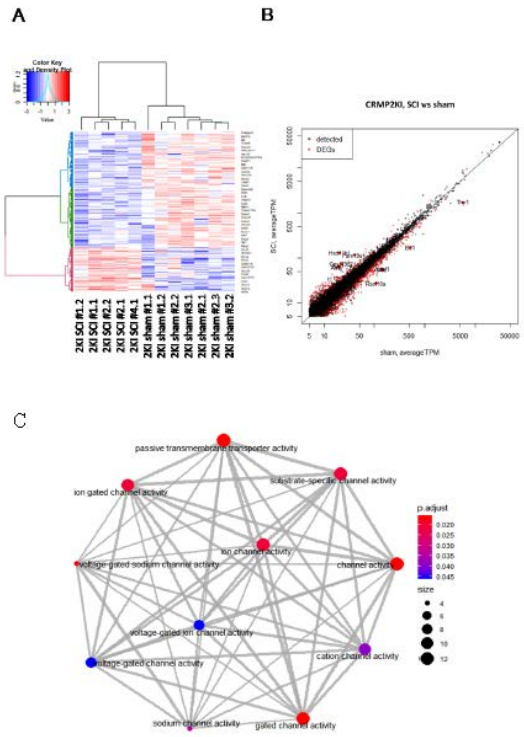

Additional Figure 3 Transcriptome analysis after spinal cord injury in CRMP2KI.

Bioinformatic analysis of DEGs after SCI in CRMP2KI mice. (A) Heatmap of all DEGs. (B) All the genes analyzed were plotted by transcripts per million (TPM) values. Red represents DEGs and black represents detected genes. Gene names indicate top 5 up- or down-regulated genes. (C) GO enrichment analysis of upregulated genes. Only molecular function terms were detected. Each dot represents one GO term and the thickness of lines shows the number of shared genes between two GO terms. CRMP2: Collapsin response mediator protein 2; DEGs: differentially expressed genes; KI: knock-in; SCI: spinal cord injury.

Additional Table 2 Enriched pathways of downregulated DEGs by the phosphorylation deficient of CRMP2 (P<0.05, q<0.2)

Database	Description	Ratio of DEGs	Ratio of universe	P-value	P adjust	q-value	Gene name
KEGG	Biosynthesis of unsaturated fatty acids	8/175	21/4117	1.15E-06	0.000236049	0.000232715	Elovl6/Hsd17b4/Fads2/Elovl4/Scd1/Fads1/Hsd17b12/Hacd3
KEGG	Lysosome	15/175	98/4117	1.22E-05	0.00089044	0.000877866	Gla/Man2b1/Entpd4/Gm2a/Acp2/Entpd4/Entpd4b/Scarb2/Lamp2/Hexa/Asah1/Gns/Lgmn/Smpd1/Ctsd/Ctsb
KEGG	Fatty acid metabolism	10/175	45/4117	1.30E-05	0.00089044	0.000877866	Elovl6/Acsl1/Hsd17b4/Acaa2/Fads2/Elovl4/Scd1/Fads1/Hsd17b12/Hacd3
GO	lysosome	29/455	304/11442	1.14E-05	0.002429124	0.002071406	Gla/Rptor/Man2b1/Gm2a/Acp2/Psen1/Slc35f6/Scarb2/Bace1/Snx14/Rnaset2a/Ncstn/Lamp2/Hexa/Plbd2/Asah1/Gns/Ostm1/Ank3/Pon2/Mlc1/Gja1/Lgmn/Smpd1/Rnf13/Arl8b/Ctsd/Ctsb/Rab7
GO	lytic vacuole	29/455	305/11442	1.21E-05	0.002429124	0.002071406	Gla/Rptor/Man2b1/Gm2a/Acp2/Psen1/Slc35f6/Scarb2/Bace1/Snx14/Rnaset2a/Ncstn/Lamp2/Hexa/Plbd2/Asah1/Gns/Ostm1/Ank3/Pon2/Mlc1/Gja1/Lgmn/Smpd1/Rnf13/Arl8b/Ctsd/Ctsb/Rab7
GO	vacuole	33/455	374/11442	1.47E-05	0.002429124	0.002071406	Gla/Rptor/Abcb6/Man2b1/Entpd4/Gm2a/Acp2/Psen1/Entpd4b/Slc35f6/Scarb2/Bace1/Snx14/Rnaset2a/Ncstn/Lamp2/Hexa/Plbd2/Asah1/Gns/Ostm1/Ank3/Pon2/Atg12/Mlc1/Gja1/Lgmn/Smpd1/Rnf13/Arl8b/Ctsd/Ctsb/Rab7
GO	GABA-ergic synapse	12/455	88/11442	0.000178214	0.020677491	0.017632481	Gabrb1/Slitrk3/Iqsec3/Gabrb2/Nlgn3/Gucy1a1/Rims2/Cdh13/Clstn3/Sv2a/Pak1/Atp2b1
GO	neuromuscular junction	11/455	78/11442	0.000243901	0.020677491	0.017632481	Camk2d/Unc13a/Psen1/Dnaja3/Dlg2/Ank3/Dnajc5/Stx1b/Serpine2/Sv2a/Syp
GO	endoplasmic reticulum subcompartment	31/455	397/11442	0.000257064	0.020677491	0.017632481	Faf1/Pnpt1/Derl2/Ero1l/Fmn2/Elovl6/Rdh11/Cant1/Mmgt1/Slc35b4/Dnajc18/Dhcr7/Rnf121/Svip/Emc1/Ncln/Ptdss1/Derl1/Elovl4/Spcs3/Cyb5r3/Scd1/Cds2/Slc9a6/Nos1ap/Reep1/Calr/Canx/Vapa/Rab18/Abhd12
GO	nuclear outer membrane-endoplasmic reticulum membrane network	31/455	402/11442	0.000319842	0.020677491	0.017632481	Faf1/Pnpt1/Derl2/Ero1l/Fmn2/Elovl6/Rdh11/Cant1/Mmgt1/Slc35b4/Psen1/Dnajc18/Dhcr7/Rnf121/Svip/Emc1/Ncln/Ptdss1/Derl1/Elovl4/Spcs3/Cyb5r3/Scd1/Cds2/Slc9a6/Nos1ap/Reep1/Calr/Canx/Vapa/Abhd12
GO	endoplasmic reticulum membrane	30/455	385/11442	0.000334182	0.020677491	0.017632481	Faf1/Pnpt1/Derl2/Ero1l/Fmn2/Elovl6/Rdh11/Cant1/Mmgt1/Slc35b4/Dnajc18/Dhcr7/Rnf121/Svip/Emc1/Ncln/Ptdss1/Derl1/Elovl4/Spcs3/Cyb5r3/Scd1/Cds2/Slc9a6/Nos1ap/Reep1/Calr/Canx/Vapa/Abhd12
GO	plasma membrane protein complex	27/455	336/11442	0.000407715	0.022424323	0.01912207	Chrna4/Cdh20/Nlgn1/Pmp22/Gng4/Kcna1/Cdh22/Eps15l1/Lin7a/Psen1/Cntfr/Cdh11/Kcng1/Ap2a2/Ncstn/Coro1c/Cdh13/Gng7/Kcnf1/Dlg2/Dpp6/Tmed10/Grin1/Nos1ap/Gja1/Atp1b2/Abhd12
GO	presynapse	33/455	455/11442	0.000618671	0.026878662	0.022920454	Dgkq/Chrna4/Exoc4/Rnf40/Rab8b/Flrt3/D230025D16Rik/Unc13a/Kcna1/Psen1/Slc29a1/Bace1/Rims2/Polg/Ap2a2/Ncstn/Adcyap1/Slc9a6/Dnajc5/Grin1/Nos1ap/Ncam1/Kif1a/Stx1b/Lgi3/Rapgef4/Canx/Dpysl2/Sv2a/Rab7/Atp2b1/Mff/Syp
GO	synaptic membrane	31/455	419/11442	0.000647352	0.026878662	0.022920454	Nrp1/Chrna4/Gabrb1/Dlgap2/Slitrk3/Flrt3/Nlgn1/Unc13a/Iqsec3/Kcna1/Gabrb2/Arrb1/Lin7a/Psen1/Nlgn3/Rims2/Syne1/Ncstn/Dnaja3/Syt3/Dlg2/Ank3/Grin1/Ncam1/Stx1b/Clstn3/Canx/Nrcam/Fabp5/Atp2b1/Syp
GO	ciliary rootlet	4/455	11/11442	0.000651604	0.026878662	0.022920454	Psen1/Kif5b/Kif5c/Kif5a
GO	axon part	28/455	369/11442	0.000794758	0.029303394	0.024988115	Nrp1/Exoc4/Rnf40/Flrt3/Camk2d/Unc13a/Kcna1/Psen1/Polg/Adcyap1/Agrn/Dlg2/Ank3/Slc9a6/Kif5b/Epb41l3/Grin1/Ncam1/Fgf13/Rapgef4/Nrcam/Dpysl2/Kif5c/Map1b/Pak1/Kif5a/Syp/Nrsn1
GO	integral component of synaptic membrane	17/455	180/11442	0.000828783	0.029303394	0.024988115	Nrp1/Chrna4/Slitrk3/Flrt3/Nlgn1/Kcna1/Gabrb2/Psen1/Nlgn3/Ncstn/Syt3/Grin1/Ncam1/Clstn3/Canx/Nrcam/Atp2b1
GO	intrinsic component of synaptic membrane	18/455	198/11442	0.000921604	0.030142836	0.025703939	Nrp1/Chrna4/Slitrk3/Flrt3/Nlgn1/Kcna1/Gabrb2/Psen1/Nlgn3/Ncstn/Syt3/Dlg2/Grin1/Ncam1/Clstn3/Canx/Nrcam/Atp2b1
GO	lateral plasma membrane	6/455	30/11442	0.001006775	0.030142836	0.025703939	Prickle2/Cldn12/Coro1c/Ank3/Gja1/Fgf13
GO	exocytic vesicle	18/455	200/11442	0.001035209	0.030142836	0.025703939	Exoc4/Rab8b/D230025D16Rik/Unc13a/Psen1/Bace1/Ap2a2/Ncstn/Syt3/Dnajc5/Grin1/Kif1a/Stx1b/Lgi3/Sv2a/Rab7/Mff/Syp
GO	secretory vesicle	26/455	341/11442	0.001129942	0.031073399	0.026497465	Exoc4/Rab8b/D230025D16Rik/Unc13a/Psen1/Bace1/Ap2a2/Ncstn/Lamp2/Hexa/Syt3/Dnajc5/Tmed10/Grin1/Kif1a/Stx1b/Lgi3/Smpd1/Calr/Serpine2/Scg3/Sv2a/Scg2/Rab7/Mff/Syp
GO	endoplasmic reticulum part	33/455	476/11442	0.001331243	0.034682373	0.029574975	Faf1/Pnpt1/Derl2/Ero1l/Pdia4/Fmn2/Elovl6/Rdh11/Cant1/Mmgt1/Slc35b4/Dnajc18/Dhcr7/Rnf121/Svip/Emc1/Rnaset2a/Ncln/Ptdss1/Derl1/Elovl4/Spcs3/Cyb5r3/Scd1/Cds2/Slc9a6/Nos1ap/Reep1/Calr/Canx/Vapa/Rab18/Abhd12
GO	synaptic vesicle	17/455	189/11442	0.001423034	0.035220098	0.030033513	Exoc4/Rab8b/D230025D16Rik/Unc13a/Psen1/Bace1/Ap2a2/Ncstn/Dnajc5/Grin1/Kif1a/Stx1b/Lgi3/Sv2a/Rab7/Mff/Syp
GO	intrinsic component of postsynaptic membrane	14/455	143/11442	0.00165612	0.038972408	0.03323325	Nrp1/Chrna4/Slitrk3/Flrt3/Nlgn1/Kcna1/Gabrb2/Nlgn3/Dlg2/Grin1/Ncam1/Clstn3/Canx/Nrcam
GO	transport vesicle	21/455	263/11442	0.00188892	0.038972408	0.03323325	Exoc4/Rab8b/D230025D16Rik/Unc13a/Psen1/Bace1/Ap2a2/Ncstn/Klhl12/Syt3/Tgoln1/Dnajc5/Grin1/Kif1a/Stx1b/Lgi3/Sv2a/Rab7/Mff/Syp/Nrsn1
GO	outer membrane	14/455	145/11442	0.001889571	0.038972408	0.03323325	Abcb6/Acsl1/Psen1/Dhcr7/Armcx3/Cyb5r3/Tomm70a/Miga2/Mfn2/Cyb5b/Acsl6/Pgam5/Gja1/Mff
GO	organelle outer membrane	14/455	145/11442	0.001889571	0.038972408	0.03323325	Abcb6/Acsl1/Psen1/Dhcr7/Armcx3/Cyb5r3/Tomm70a/Miga2/Mfn2/Cyb5b/Acsl6/Pgam5/Gja1/Mff
GO	cell surface	30/455	430/11442	0.001979516	0.039194419	0.033422567	Nrp1/Pdia4/Chrna4/Cdh20/Cx3cr1/Nlgn1/Pmp22/Kcna1/Cdh22/Psen1/Cntfr/Nlgn3/Cdh11/Bace1/Tspan14/Cxcl12/Sdc4/Cdh13/Cd99l2/Agrn/Dpp6/Ank3/Grin1/Ncam1/Slc1a3/Cd200/Calr/Clstn3/Serpine2/Ctsb
GO	distal axon	23/455	302/11442	0.002174128	0.041392052	0.035296571	Nrp1/Exoc4/Rnf40/Flrt3/Unc13a/Kcna1/Psen1/Polg/Adcyap1/Agrn/Slc9a6/Kif5b/Grin1/Ncam1/Fgf13/Rapgef4/Dpysl2/Kif5c/Map1b/Pak1/Kif5a/Syp/Nrsn1
GO	postsynaptic membrane	23/455	304/11442	0.002365354	0.042970759	0.036642795	Nrp1/Chrna4/Gabrb1/Dlgap2/Slitrk3/Flrt3/Nlgn1/Iqsec3/Kcna1/Gabrb2/Arrb1/Lin7a/Nlgn3/Syne1/Dnaja3/Dlg2/Ank3/Grin1/Ncam1/Clstn3/Canx/Nrcam/Fabp5
GO	vacuolar membrane	13/455	133/11442	0.002430669	0.042970759	0.036642795	Abcb6/Man2b1/Entpd4/Psen1/Entpd4b/Slc35f6/Scarb2/Ncstn/Lamp2/Rnf13/Arl8b/Ctsd/Rab7
GO	integral component of postsynaptic membrane	13/455	134/11442	0.002597208	0.044331657	0.037803284	Nrp1/Chrna4/Slitrk3/Flrt3/Nlgn1/Kcna1/Gabrb2/Nlgn3/Grin1/Ncam1/Clstn3/Canx/Nrcam
GO	growth cone	16/455	184/11442	0.002741166	0.04522924	0.038568687	Nrp1/Exoc4/Flrt3/Psen1/Agrn/Kif5b/Grin1/Ncam1/Fgf13/Rapgef4/Dpysl2/Kif5c/Map1b/Pak1/Kif5a/Nrsn1
GO	site of polarized growth	16/455	185/11442	0.00289416	0.045762058	0.039023042	Nrp1/Exoc4/Flrt3/Psen1/Agrn/Kif5b/Grin1/Ncam1/Fgf13/Rapgef4/Dpysl2/Kif5c/Map1b/Pak1/Kif5a/Nrsn1
GO	vacuolar part	13/455	136/11442	0.002958355	0.045762058	0.039023042	Abcb6/Man2b1/Entpd4/Psen1/Entpd4b/Slc35f6/Scarb2/Ncstn/Lamp2/Rnf13/Arl8b/Ctsd/Rab7
KEGG	Fatty acid elongation	5/175	19/4117	0.000937219	0.04803246	0.047354209	Elovl6/Acaa2/Elovl4/Hsd17b12/Hacd3
Hallmark	KRAS_SIGNALING_UP	14/148	125/3054	0.002444392	0.062081395	0.060014238	Ero1l/Tmem176a/Nrp1/Gucy1a1/Spon1/Rbm4/Hsd11b1/Fgf9/Etv5/Ank/Epb41l3/Kif5c/Scg3/Tspan13
Hallmark	EPITHELIAL_MESENCHYMAL_TRANSITION	13/148	112/3054	0.002533934	0.062081395	0.060014238	Fstl1/Timp3/Pmp22/Tpm4/Cdh11/Cxcl12/Sdc4/Edil3/Copa/Gja1/Htra1/Serpine2/Scg2
Reactome	Metabolism of lipids	33/238	397/5641	0.000109589	0.064767256	0.062984989	Pnpla2/Mtmr14/Fig4/Elovl6/Cyp2d22/Acsl1/Gm2a/Srebf1/Hsd17b4/Gpd2/Acaa2/Dhcr7/Agpat3/Hsd11b1/Ptdss1/Fads2/Hexa/Asah1/Osbpl2/Abhd4/Pitpnb/Miga2/Pon2/Scd1/Cds2/Fads1/Acsl6/Hsd17b12/Hacd3/Smpd1/Chd9/Vapa/Fabp5
Reactome	Synthesis of very long-chain fatty acyl-CoAs	5/238	17/5641	0.000522718	0.107810742	0.104844002	Elovl6/Acsl1/Acsl6/Hsd17b12/Hacd3
Reactome	Neuronal System	23/238	261/5641	0.000573783	0.107810742	0.104844002	Chrna4/Gabrb1/Dlgap2/Slitrk3/Kcnj16/Camk2d/Nlgn1/Gng4/Kcna1/Gabrb2/Lin7a/Nlgn3/Kcng1/Ap2a2/Slc38a1/Kcnf1/Dlg2/Slc1a1/Abat/Dnajc5/Epb41l3/Grin1/Slc1a3
Reactome	Neutrophil degranulation	25/238	300/5641	0.000761129	0.107810742	0.104844002	Man2b1/Cant1/Gm2a/Psen1/Pdxk/Tspan14/Svip/Rnaset2a/Ap2a2/Ncstn/Lamp2/Asah1/Pygb/Gns/Rab31/Cyb5r3/Dnajc5/Vapa/Fabp5/Rab18/Ctsd/Psmb1/Ctsb/Rab7/Pgrmc1
Reactome	Fatty acyl-CoA biosynthesis	6/238	28/5641	0.000912104	0.107810742	0.104844002	Elovl6/Acsl1/Scd1/Acsl6/Hsd17b12/Hacd3
Reactome	Peptide hormone metabolism	6/238	29/5641	0.001110059	0.109340797	0.106331953	Ero1l/Exoc4/Pcsk1/Spcs3/Pla2g7/Ctsd
KEGG	PPAR signaling pathway	6/175	35/4117	0.003141715	0.128810307	0.126991419	Acsl1/Fads2/Slc27a1/Scd1/Fabp5/Ubc

Reactome	Transport of small molecules	28/238	373/5641	0.001870321	0.157908545	0.153563212	Derl2/Abcb6/Atp13a1/Ano10/Camk2d/Gng4/Clcn6/Slc20a2/Slc35b4/Slc29a1/Slco1c1/Nipa2/Ap2a2/Slc6a15/Derl1/Slc38a1/Slc27a1/Eif2s3x/Ostm1/Pmpca/Slc9a6/Pex19/Ank/Tsc22d3/Atp1b2/Ubc/Atp2b1/Atp6v0e2
Reactome	N-glycan trimming in the ER and Calnexin/Calreticulin cycle	5/238	23/5641	0.002309836	0.17063917	0.165943515	Derl2/Derl1/Calr/Canx/Ubc
Reactome	Transmission across Chemical Synapses	15/238	159/5641	0.002726609	0.179047339	0.174120308	Chrna4/Gabrb1/Kcnj16/Camk2d/Gng4/Gabrb2/Lin7a/Ap2a2/Slc38a1/Dlg2/Slc1a1/Abat/Dnajc5/Grin1/Slc1a3
Hallmark	HEDGEHOG_SIGNALING	5/148	29/3054	0.011549298	0.188638529	0.182357332	Nrp1/Cntfr/Nrcam/Dpysl2/Scg2

Additional Table 3 Top20 significantly upregulated DEGs by the phosphorylation deficient of CRMP2

	Gene	Molecular Function GO term	Cellular Component GO term	Biological Process GO term	WT average TPM	CRMP2KI average TPM	*P*-value	FC	log2FC	Average z-score	WT SCI *vs*. sham	2KI SCI *vs*. sham
1	Gm17494	-	-	-	24.02	264.15	0.0006	11.00	3.46	21.34	FC0.03	FC0.97
2	Gm6166	-	-	-	21.10	170.67	0.0006	8.09	3.02	15.08	FC1.28	FC0.87
3	Scn2b	transmembrane transporter activity	plasma membrane, protein-containing complex	transmembrane transport, circulatory system process, homeostatic process, aatomical structure development	15.80	109.67	0.0023	6.94	2.80	13.72	FC1.51	FC0.90
4	mt-Ts2	-	-	-	13.21	86.96	0.0262	6.58	2.72	12.88	FC1.67	FC1.72
5	Ndufa11	protein-containing complex	mitochondrion, cytoplasm, intracellular	mitochondrion organization, protein-containing complex assembly, cellular component assembly	104.26	550.52	0.0006	5.28	2.40	10.30	↑ FC1.35	↓ FC0.71
6	Pi4ka	kinase activity	plasma membrane, cytoplasm, cell	lipid metabolic process, signal transuction, membran organization, symbiont process	36.21	190.77	0.0006	5.27	2.40	9.84	↑ FC1.31	FC0.96
7	Gm3375	-	-	-	43.10	225.24	0.0006	5.23	2.39	9.75	↑ FC1.19	FC0.87
8	Tnnc1	ion/cytoskeletal protein binding	cytoskeleton, cytoplasm, protein-containing complex	circulatory system process, anatomical strcture development, transport	23.14	98.82	0.0023	4.27	2.09	6.87	FC1.85	FC0.50
9	Gm47441	-	-	-	26.52	111.16	0.0012	4.19	2.07	6.70	↑ FC2.61	FC0.64
10	Hpcal4	ion binding	-	signal transduction	22.58	93.75	0.0006	4.15	2.05	6.61	FC1.15	↓ FC0.45
11	Snhg9	-	-	-	9.33	36.17	0.0317	3.88	1.95	5.68	FC1.26	FC0.26
12	AC149090	lyase activity	-	lipid metabolic process, biosynthetic process	47.36	164.04	0.0006	3.46	1.79	5.59	↑ FC1.30	FC0.99
13	Gm10012	-	-	-	34.52	113.45	0.0006	3.29	1.72	5.17	FC1.07	↓ FC0.64
14	Gpatch11	protein-contaiing complex	cromosome, inracellular	-	8.17	29.05	0.0006	3.55	1.83	5.01	FC1.08	FC0.63
15	Gm48016	-	-	-	14.24	45.70	0.0012	3.21	1.68	5.00	↑ FC2.45	FC0.63
16	Tomm6	protein-containing complex	cytoplasm,mitochondrion	transport, protein transport	90.61	287.59	0.0041	3.17	1.67	4.76	FC0.97	↓ FC0.49
17	Mrpl52	structural constituent of ribosome, structural molecule activity	ribosome,mitochondrion,cytoplasm, protein-containing complex	translation, biosynthetic process, cellular nitrogen compound metabolic process	57.12	162.83	0.0006	2.85	1.51	4.29	↑ FC1.37	FC0.83
18	Kctd1	transcription factor binding	nucleus, intracellular	cellular nitrogen compound metabolic process, biosynthetic process, protein-containing complex assembly	9.35	29.50	0.0006	3.16	1.66	4.20	FC1.81	FC0.46
19	Gm4544	-	-	-	7.50	25.31	0.0159	3.37	1.75	4.09	FC1.91	↓ FC0.25
20	Pagr1a	transcription factor binding, protein-containing complex	nucleus, nucleoplasm, intracellular	DNA metabilic process, chromosom organization, signal transduction, cell cycle, immune system process, response to stress, biosynthetic process	7.38	28.47	0.0350	3.86	1.95	4.08	FC1.61	FC1.13

FC between other condition in cortex layer Ⅴ were shown together. ↑ ↓ arrows show the genes were DEGs in the other conditional comparisons.

Additional Table 4 Top20 significantly downregulated DEGs by the phosphorylation deficient of CRMP2

	Gene	Molecular Function GO term	Cellular Component GO term	Biological Process GO term	WT average TPM	CRMP2KI average TPM	*P*-value	FC	log2FC	Average z-score	WT SCI vs sham	2KI SCI vs sham
1	CT010467.1	-	-	-	153.60	34.48	0.0006	0.22	-2.16	-2.75	FC0.97	FC1.89
2	Gm10800	-	-	-	378.28	101.20	0.0041	0.27	-1.90	-2.51	FC1.11	FC1.38
3	Rab18	ion binding, GTPase activity	Golgi apparatus, enoplasmic reticlum, plasma membrane	protein transport, anatomical structure development, signal transduction, nucleocytoplasmic transport	167.20	54.47	0.0006	0.33	-1.62	-2.46	FC0.94	FC1.00
4	Ubc	enzyme binding	nucleus, nucleoplasm, cytosol	cellular protein modification process, catabolic process	439.88	133.63	0.0006	0.30	-1.72	-2.38	FC1.06	FC1.06
5	Malat1	-	-	-	216.98	82.10	0.0111	0.38	-1.40	-2.30	FC0.79	↑ FC1.54
6	Dpysl2	cytoskeletal protein binding, hydrolase activity, enzyme binding	cytoskeleton, mitochondrion, plasma membrane, cytosol	cytoskeleton organization, cell differentiation/morphogenesis, growth, vesicle-mediated transport	208.93	81.54	0.0006	0.39	-1.36	-2.27	FC0.92	↑ FC1.34
7	mt-Tm	-	-	-	1771.70	735.53	0.0070	0.42	-1.27	-2.25	FC0.68	↑ FC1.48
8	Nrcam	cytoskeletal protein binding	plasma membrane, extracellular region, cell, organelle	nervous system process, cell differentiation/adhesion/morphogenesis, anatomical structure formation involved in morphogenesis, locomotion	163.51	69.02	0.0023	0.42	-1.24	-2.17	FC0.96	FC1.46
9	Gm23374	-	-	-	33.32	6.65	0.0006	0.20	-2.32	-2.10	FC1.01	FC1.11
10	Ggt7	peptidase activity, transferase activity	cell, plasma membrane	cellular nitrogen compound metabolic/sulfur compound metabolic/biosynthetic process, translation, response to stress	98.00	20.45	0.0006	0.21	-2.26	-2.10	FC1.13	FC1.29
11	Gm7292	-	-	-	72.06	16.53	0.0006	0.23	-2.12	-2.05	FC0.78	FC0.54
12	Gm10222	-	-	-	4266.41	945.81	0.0006	0.22	-2.17	-2.03	↓ FC0.78	FC2.54
13	Map1b	cytoskeletal protein/ion/lipid binding	cytoskeleton, cilium, plasma membrane, cytoplasm	cytoskeleton organization, cell differentiation/morphogenesis, intracellular transport, response to stress, cell-cell signaling	189.34	91.18	0.0006	0.48	-1.05	-2.00	↓ FC0.73	FC1.07
14	Vapa	cytoskeletal protein binding	nucleus, Golgi apparatus, endoplasmic reticulum, nuclear envelope, cytoskeleton	(vesicle-mediated) transport, anatomical structure development, cell death, symboint process, membrane organization	238.47	126.54	0.0023	0.53	-0.91	-1.86	FC1.07	FC1.03
15	Trp53i11	-	-	-	25.50	5.53	0.0041	0.22	-2.21	-1.85	FC0.60	FC1.39
16	Gm17922	-	-	-	68.01	21.65	0.0041	0.32	-1.65	-1.85	↓ FC0.56	↑ FC3.45
17	Agrn	ion binding, structural molecule actibity, enzyme regulator activity	Golgi apparatus, extracellular matrix, plasa membrane, cytoplasm	celular protein modification process, biosynthetic process,anatomical structure development, cell differentiation, transmembrane transport, cytoskeleton organization, membrane organization, cell-cell signaling	34.30	11.04	0.0070	0.32	-1.64	-1.81	FC0.84	FC0.98
18	mt-Tl1	-	-	-	780.27	419.71	0.0070	0.54	-0.89	-1.81	FC0.72	FC1.08
19	2900097C17Rik	-	-	-	516.48	279.28	0.0070	0.54	-0.89	-1.80	FC0.93	FC0.65
20	B230209E15Rik	-	-	-	57.58	22.06	0.0023	0.38	-1.38	-1.78	FC1.02	FC1.24

FC between other condition in cortex layer V were shown together. ↑ ↓ arrows show the genes were DEGs in the other conditional comparisons.

Additional Table 5 Enriched pathways of upregulated DEGs after spinal cord injury in WT ($P < 0.05$, $q < 0.05$)

Database	Description	Ratio of DEGs	Ratio of	*P*-value	*P* adjust	*q* value	gene name
GO	ribosomal subunit	87/755	214/12262	1.03E-49	4.61E-47	4.20E-47	Gm6576/Gm10036/Gm5786/Mrps28/Gm9493/Rpl13-ps3/Rpl7l1/Mrpl10/Mrpl44/Rps20/Mrpl51/Mrps11/Mpv17l2/Mrps7/Gm10020/Gm10073/Mrpl2/Mrpl52/Rpl22/Mrpl4/Mrps24/Zcchc17/Rpl28/Mrpl34/Rpl29/Mrps36/Rpl9-ps6/Hba-a2/Hba-a1/Rpl23a-ps3/Rpl15/Rack1/Mrps18a/Mrpl28/Rpl10a/Mrpl12/Rpl18/Rpl35a/Mrpl41/Mrps12/Rpl36a/Rps9/Rps18/Rps5/Rps27a/Rps24/Rplp2/Rpl14/Mrpl30/Rps6/Rpl6/Rps3/Rps4x/Rpsa/Rpl7/Rpl27a/Rps23/Rps10/Mrps21/Rpl36/Rpl30/Rps17/Mrpl42/Rpl35/Rpl27/Rplp0/Rps28/Rpl31/Rpl39/Rps13/Rpl13/Rps11/Rpl8/Rps3a1/Fau/Rpl9/Rpl3/Rpl26/Rps15/Rpl13a/Uba52/Rpl24/Rpl19/Rps14/Rpl4/Rps27/Rplp1
GO	ribosome	93/755	248/12262	1.67E-49	4.61E-47	4.20E-47	Gm6576/Pnpt1/Gm10036/Gm5786/Mrps28/Gm9493/Rpl13-ps3/Rpl7l1/Mrpl10/Mrpl44/Rps20/Mrpl51/Mrps11/Mpv17l2/Mrps7/Gm10020/Gm10073/Mrpl2/Mrpl52/Rpl22/Mrpl4/Mrps24/Zcchc17/Rpl28/Mrpl34/Rpl29/Mrps36/Rpl9-ps6/Hba-a2/Hba-a1/Rpl23a-ps3/Rpl15/Rack1/Eif3h/Mrps18a/Mrpl28/Mrps33/Rpl10a/Mrpl12/Rpl18/Rpl35a/Btf3/Mrpl41/Mrps12/Rpl36a/Rps9/Rps18/Rps5/Rps27a/Rps24/Rplp2/Rpl14/Mrpl30/Rps6/Rpl6/Rps3/Rps4x/Rpsa/Rpl7/Rpl27a/Rps23/Rps10/Mrps21/Rpl36/Rpl30/Rps17/Mrpl42/Rpl35/Rpl27/Rplp0/Rps28/Rpl31/Rpl39/Rps13/Rpl13/Rps11/Rpl8/Rps3a1/Fau/Rpl9/Rpl3/Rpl26/Rps15/Rpl13a/Uba52/Rpl41/Rpl24/Rpl19/Rps14/Rpl4/Ndufa7/Rps27/Rplp1
GO	structural constituent of ribosome	76/733	169/11958	1.65E-47	1.16E-44	1.12E-44	Gm6576/Gm10036/Gm5786/Rpl7l1/Mrpl10/Rps20/Mrpl51/Mrps11/Mrps7/Gm10020/Gm10073/Mrpl2/Mrpl52/Rpl22/Mrpl4/Mrps24/Rpl28/Mrpl34/Rpl29/Rpl9-ps6/Rpl23a-ps3/Rpl15/Mrps18a/Mrpl28/Rpl10a/Mrpl12/Rpl18/Rpl35a/Mrpl41/Mrps12/Rps9/Rps18/Rps5/Rps27a/Rps24/Rplp2/Rpl14/Mrpl30/Rps6/Rpl6/Rps3/Rps4x/Rpsa/Rpl7/Rpl27a/Rps23/Rps10/Mrps21/Rpl36/Rpl30/Rps17/Rpl35/Rpl27/Rplp0/Rps28/Rpl31/Rpl39/Rps13/Rpl13/Rps11/Rpl8/Rps3a1/Fau/Rpl9/Rpl3/Rpl26/Rps15/Rpl13a/Rpl41/Rpl24/Rpl19/Rps14/Rpl4/Ndufa7/Rps27/Rplp1
GO	cytosolic ribosome	66/755	132/12262	6.86E-45	1.26E-42	1.15E-42	Gm6576/Gm10036/Gm5786/Gm9493/Rpl13-ps3/Rpl7l1/Rps20/Gm10020/Gm10073/Rpl22/Zcchc17/Rpl28/Rpl29/Rpl9-ps6/Hba-a2/Hba-a1/Rpl23a-ps3/Rpl15/Rack1/Rpl10a/Rpl18/Rpl35a/Rpl36a/Rps9/Rps18/Rps5/Rps27a/Rps24/Rplp2/Rpl14/Rps6/Rpl6/Rps3/Rps4x/Rpsa/Rpl7/Rpl27a/Rps23/Rps10/Rpl36/Rpl30/Rps17/Rpl35/Rpl27/Rplp0/Rps28/Rpl31/Rpl39/Rps13/Rpl13/Rps11/Rpl8/Rps3a1/Fau/Rpl9/Rpl3/Rpl26/Rps15/Rpl13a/Uba52/Rpl24/Rpl19/Rps14/Rpl4/Rps27/Rplp1
Reactome	Formation of a pool of free 40S subunits	56/419	93/5985	6.95E-42	5.03E-39	4.49E-39	Eif3b/Rps20/Rpl22/Rpl28/Eif3f/Rpl29/Eif3g/Rpl15/Eif3h/Rpl18/Rpl35a/Eif3i/Rpl36a/Rps9/Rps18/Rps5/Rps27a/Rps24/Rplp2/Rpl14/Rps6/Rpl6/Rps3/Rps4x/Rpsa/Rpl7/Rpl27a/Rps23/Rpl36al/Rps10/Eif3k/Rpl30/Rps17/Rpl35/Rpl27/Rplp0/Rps28/Rpl31/Rpl39/Rps13/Rpl13/Rps11/Rpl8/Rps3a1/Rpl9/Rpl3/Rpl26/Rps15/Rpl13a/Uba52/Rpl24/Rpl19/Rps14/Rpl4/Rps27/Rplp1
Reactome	Translation	81/419	215/5985	1.89E-40	6.83E-38	6.09E-38	Eif2b3/Mrrf/Mrps28/Eif3b/Mrpl10/Srp68/Mrpl44/Rps20/Mrpl51/Mrps7/Mrpl2/Mrpl52/Rpl22/Mrpl4/Mrps24/Rpl28/Eif3f/Mrpl34/Rpl29/Mrps36/Eif3g/Rpl15/Eif3h/Mrps18a/Mrpl28/Mrps33/Mrpl12/Rpl18/Rpl35a/Eif3i/Mrpl41/Mrps12/Rpl36a/Rps9/Rps18/Rps5/Rps27a/Rps24/Rplp2/Rpl14/Mrpl30/Rps6/Rpl6/Rps3/Rps4x/Rpsa/Rpl7/Rpl27a/Rps23/Rpl36al/Rps10/Eif3k/Mrps21/Rpl30/Rps17/Mrpl42/Rpl35/Rpl27/Rplp0/Rps28/Eef1g/Rpl31/Rpl39/Rps13/Rpl13/Rps11/Rpl8/Srp14/Rps3a1/Rpl9/Rpl3/Rpl26/Rps15/Rpl13a/Uba52/Rpl24/Rpl19/Rps14/Rpl4/Rps27/Rplp1
Reactome	SRP-dependent cotranslational protein targeting to membrane	52/419	83/5985	3.46E-40	8.36E-38	7.46E-38	Srp68/Rps20/Rpl22/Rpl28/Rpl29/Rpl15/Rpl18/Rpl35a/Rpl36a/Rps9/Rps18/Rps5/Rps27a/Rps24/Rplp2/Rpl14/Rps6/Rpl6/Rps3/Rps4x/Rpsa/Rpl7/Rpl27a/Rps23/Rpl36al/Rps10/Rpl30/Rps17/Rpl35/Rpl27/Rplp0/Rps28/Rpl31/Rpl39/Rps13/Rpl13/Rps11/Rpl8/Srp14/Rps3a1/Rpl9/Rpl3/Rpl26/Rps15/Rpl13a/Uba52/Rpl24/Rpl19/Rps14/Rpl4/Rps27/Rplp1
Reactome	L13a-mediated translational silencing of Ceruloplasmin expression	56/419	103/5985	1.70E-38	3.07E-36	2.74E-36	Eif3b/Rps20/Rpl22/Rpl28/Eif3f/Rpl29/Eif3g/Rpl15/Eif3h/Rpl18/Rpl35a/Eif3i/Rpl36a/Rps9/Rps18/Rps5/Rps27a/Rps24/Rplp2/Rpl14/Rps6/Rpl6/Rps3/Rps4x/Rpsa/Rpl7/Rpl27a/Rps23/Rpl36al/Rps10/Eif3k/Rpl30/Rps17/Rpl35/Rpl27/Rplp0/Rps28/Rpl31/Rpl39/Rps13/Rpl13/Rps11/Rpl8/Rps3a1/Rpl9/Rpl3/Rpl26/Rps15/Rpl13a/Uba52/Rpl24/Rpl19/Rps14/Rpl4/Rps27/Rplp1
KEGG	Ribosome	61/334	118/4389	1.48E-38	3.74E-36	3.74E-36	Mrpl10/Rps20/Mrps7/Mrpl2/Rpl22/Mrpl4/Rpl28/Mrpl34/Rpl29/Gm8210/Rpl15/Mrps18a/Mrpl28/Mrpl12/Rpl18/Rpl35a/Mrps12/Rpl36a/Rpl36al/Rps9/Rps18/Rps5/Rps27a/Rps24/Rplp2/Rpl14/Mrpl30/Rps6/LOC105244208/Rpl6/Rps3/Rps4x/Rpsa/Rpl7/Rpl27a/Rps23/Rps10/Mrps21/Rpl36/Rpl30/Rps17/Rpl35/Rpl27/LOC108167922/Rplp0/Rps28/Rpl31/Rpl39/Rps13/Rpl13/Rps11/Rpl8/Rps3a1/Fau/Rpl9/Rpl3/Rpl26/Rpl13a/Uba52/Rpl41/Rpl24/Rps14/Rpl4/Rps27/Rps27rt/Rplp1
Reactome	GTP hydrolysis and joining of the 60S ribosomal subunit	56/419	104/5985	3.45E-38	5.00E-36	4.46E-36	Eif3b/Rps20/Rpl22/Rpl28/Eif3f/Rpl29/Eif3g/Rpl15/Eif3h/Rpl18/Rpl35a/Eif3i/Rpl36a/Rps9/Rps18/Rps5/Rps27a/Rps24/Rplp2/Rpl14/Rps6/Rpl6/Rps3/Rps4x/Rpsa/Rpl7/Rpl27a/Rps23/Rpl36al/Rps10/Eif3k/Rpl30/Rps17/Rpl35/Rpl27/Rplp0/Rps28/Rpl31/Rpl39/Rps13/Rpl13/Rps11/Rpl8/Rps3a1/Rpl9/Rpl3/Rpl26/Rps15/Rpl13a/Uba52/Rpl24/Rpl19/Rps14/Rpl4/Rps27/Rplp1
Reactome	Eukaryotic Translation Initiation	57/419	111/5985	2.36E-37	2.44E-35	2.18E-35	Eif2b3/Eif3b/Rps20/Rpl22/Rpl28/Eif3f/Rpl29/Eif3g/Rpl15/Eif3h/Rpl18/Rpl35a/Eif3i/Rpl36a/Rps9/Rps18/Rps5/Rps27a/Rps24/Rplp2/Rpl14/Rps6/Rpl6/Rps3/Rps4x/Rpsa/Rpl7/Rpl27a/Rps23/Rpl36al/Rps10/Eif3k/Rpl30/Rps17/Rpl35/Rpl27/Rplp0/Rps28/Rpl31/Rpl39/Rps13/Rpl13/Rps11/Rpl8/Rps3a1/Rpl9/Rpl3/Rpl26/Rps15/Rpl13a/Uba52/Rpl24/Rpl19/Rps14/Rpl4/Rps27/Rplp1
Reactome	Cap-dependent Translation Initiation	57/419	111/5985	2.36E-37	2.44E-35	2.18E-35	Eif2b3/Eif3b/Rps20/Rpl22/Rpl28/Eif3f/Rpl29/Eif3g/Rpl15/Eif3h/Rpl18/Rpl35a/Eif3i/Rpl36a/Rps9/Rps18/Rps5/Rps27a/Rps24/Rplp2/Rpl14/Rps6/Rpl6/Rps3/Rps4x/Rpsa/Rpl7/Rpl27a/Rps23/Rpl36al/Rps10/Eif3k/Rpl30/Rps17/Rpl35/Rpl27/Rplp0/Rps28/Rpl31/Rpl39/Rps13/Rpl13/Rps11/Rpl8/Rps3a1/Rpl9/Rpl3/Rpl26/Rps15/Rpl13a/Uba52/Rpl24/Rpl19/Rps14/Rpl4/Rps27/Rplp1
Reactome	Nonsense Mediated Decay (NMD) independent of the Exon Junction Complex (EJC)	50/419	86/5985	2.34E-36	2.12E-34	1.89E-34	Rps20/Rpl22/Rpl28/Rpl29/Rpl15/Rpl18/Rpl35a/Rpl36a/Rps9/Rps18/Rps5/Rps27a/Rps24/Rplp2/Rpl14/Rps6/Rpl6/Rps3/Rps4x/Rpsa/Rpl7/Rpl27a/Rps23/Rpl36al/Rps10/Rpl30/Rps17/Rpl35/Rpl27/Rplp0/Rps28/Rpl31/Rpl39/Rps13/Rpl13/Rps11/Rpl8/Rps3a1/Rpl9/Rpl3/Rpl26/Rps15/Rpl13a/Uba52/Rpl24/Rpl19/Rps14/Rpl4/Rps27/Rplp1
GO	cytosolic part	77/755	251/12262	6.12E-34	8.46E-32	7.70E-32	Gm6576/Pten/Pi4k2a/Dag1/Gm10036/Gm5786/Gm9493/Rpl13-ps3/Rpl7l1/Hbb-bt/Rps20/Kxd1/Gm10020/Gm10073/Rpl22/Zcchc17/Rpl28/Pin1/Rpl29/Hbb-bs/Rpl9-ps6/Ncs1/Hba-a2/Hba-a1/Rpl23a-ps3/Rpl15/Rack1/Rpl10a/Rpl18/Rpl35a/Tcp1/Rpl36a/Rps9/Rps18/Rps5/Rps27a/Rps24/Rplp2/Rpl14/Rps6/Rpl6/Rps3/Rps4x/Rpsa/Rpl7/Rpl27a/Rps23/Rps10/Rpl36/Rpl30/Rps17/Rpl35/Rpl27/Rplp0/Rps28/Rpl31/Rpl39/Rps13/Rpl13/Rps11/Rpl8/Psmc5/Rps3a1/Fau/Rpl9/Rpl3/Rpl26/Rps15/Rpl13a/Uba52/Rpl24/Rpl19/Rps14/Rpl4/Eno1/Rps27/Rplp1
Reactome	Nonsense-Mediated Decay (NMD)	50/419	105/5985	9.18E-31	6.65E-29	5.93E-29	Rps20/Rpl22/Rpl28/Rpl29/Rpl15/Rpl18/Rpl35a/Rpl36a/Rps9/Rps18/Rps5/Rps27a/Rps24/Rplp2/Rpl14/Rps6/Rpl6/Rps3/Rps4x/Rpsa/Rpl7/Rpl27a/Rps23/Rpl36al/Rps10/Rpl30/Rps17/Rpl35/Rpl27/Rplp0/Rps28/Rpl31/Rpl39/Rps13/Rpl13/Rps11/Rpl8/Rps3a1/Rpl9/Rpl3/Rpl26/Rps15/Rpl13a/Uba52/Rpl24/Rpl19/Rps14/Rpl4/Rps27/Rplp1
Reactome	Nonsense Mediated Decay (NMD) enhanced by the Exon Junction Complex (EJC)	50/419	105/5985	9.18E-31	6.65E-29	5.93E-29	Rps20/Rpl22/Rpl28/Rpl29/Rpl15/Rpl18/Rpl35a/Rpl36a/Rps9/Rps18/Rps5/Rps27a/Rps24/Rplp2/Rpl14/Rps6/Rpl6/Rps3/Rps4x/Rpsa/Rpl7/Rpl27a/Rps23/Rpl36al/Rps10/Rpl30/Rps17/Rpl35/Rpl27/Rplp0/Rps28/Rpl31/Rpl39/Rps13/Rpl13/Rps11/Rpl8/Rps3a1/Rpl9/Rpl3/Rpl26/Rps15/Rpl13a/Uba52/Rpl24/Rpl19/Rps14/Rpl4/Rps27/Rplp1
GO	large ribosomal subunit	53/755	137/12262	3.15E-29	3.49E-27	3.17E-27	Gm10036/Rpl13-ps3/Rpl7l1/Mrpl10/Mrpl44/Mrpl51/Mpv17l2/Gm10020/Gm10073/Mrpl2/Mrpl52/Rpl22/Mrpl4/Zcchc17/Rpl28/Mrpl34/Rpl29/Rpl9-ps6/Rpl23a-ps3/Rpl15/Mrps18a/Mrpl28/Rpl10a/Mrpl12/Rpl18/Rpl35a/Mrpl41/Rpl36a/Rplp2/Rpl14/Mrpl30/Rpl6/Rpl7/Rpl27a/Rpl36/Rpl30/Mrpl42/Rpl35/Rpl27/Rplp0/Rpl31/Rpl39/Rpl13/Rpl8/Rpl9/Rpl3/Rpl26/Rpl13a/Uba52/Rpl24/Rpl19/Rpl4/Rplp1
GO	cytosolic large ribosomal subunit	39/755	76/12262	1.82E-27	1.68E-25	1.53E-25	Gm10036/Rpl13-ps3/Rpl7l1/Gm10020/Gm10073/Rpl22/Zcchc17/Rpl28/Rpl29/Rpl9-ps6/Rpl23a-ps3/Rpl15/Rpl10a/Rpl18/Rpl35a/Rpl36a/Rplp2/Rpl14/Rpl6/Rpl7/Rpl27a/Rpl36/Rpl30/Rpl35/Rpl27/Rplp0/Rpl31/Rpl39/Rpl13/Rpl8/Rpl9/Rpl3/Rpl26/Rpl13a/Uba52/Rpl24/Rpl19/Rpl4/Rplp1
Reactome	Major pathway of rRNA processing in the nucleolus and cytosol	57/419	163/5985	2.08E-26	1.16E-24	1.04E-24	Nop14/Nip7/Nob1/Emg1/Csnk1e/Rps20/Imp3/Exosc4/Rpl22/Rpl28/Rpl29/Rpl15/Rpl18/Rpl35a/Rpl36a/Rps9/Rps18/Rps5/Rps27a/Rps24/Rplp2/Rpl14/Rps6/Rpl6/Rps3/Rps4x/Rpsa/Rpl7/Rpl27a/Rps23/Rpl36al/Rps10/Rpl30/Rps17/Rpl35/Rpl27/Rplp0/Rps28/Rpl31/Rpl39/Rps13/Rpl13/Rps11/Rpl8/Rps3a1/Rpl9/Rpl3/Rpl26/Rps15/Rpl13a/Uba52/Rpl24/Rpl19/Rps14/Rpl4/Rps27/Rplp1
Reactome	rRNA processing	57/419	163/5985	2.08E-26	1.16E-24	1.04E-24	Nop14/Nip7/Nob1/Emg1/Csnk1e/Rps20/Imp3/Exosc4/Rpl22/Rpl28/Rpl29/Rpl15/Rpl18/Rpl35a/Rpl36a/Rps9/Rps18/Rps5/Rps27a/Rps24/Rplp2/Rpl14/Rps6/Rpl6/Rps3/Rps4x/Rpsa/Rpl7/Rpl27a/Rps23/Rpl36al/Rps10/Rpl30/Rps17/Rpl35/Rpl27/Rplp0/Rps28/Rpl31/Rpl39/Rps13/Rpl13/Rps11/Rpl8/Rps3a1/Rpl9/Rpl3/Rpl26/Rps15/Rpl13a/Uba52/Rpl24/Rpl19/Rps14/Rpl4/Rps27/Rplp1
Reactome	rRNA processing in the nucleus and cytosol	57/419	163/5985	2.08E-26	1.16E-24	1.04E-24	Nop14/Nip7/Nob1/Emg1/Csnk1e/Rps20/Imp3/Exosc4/Rpl22/Rpl28/Rpl29/Rpl15/Rpl18/Rpl35a/Rpl36a/Rps9/Rps18/Rps5/Rps27a/Rps24/Rplp2/Rpl14/Rps6/Rpl6/Rps3/Rps4x/Rpsa/Rpl7/Rpl27a/Rps23/Rpl36al/Rps10/Rpl30/Rps17/Rpl35/Rpl27/Rplp0/Rps28/Rpl31/Rpl39/Rps13/Rpl13/Rps11/Rpl8/Rps3a1/Rpl9/Rpl3/Rpl26/Rps15/Rpl13a/Uba52/Rpl24/Rpl19/Rps14/Rpl4/Rps27/Rplp1
GO	mitochondrial protein complex	64/755	241/12262	2.01E-24	1.59E-22	1.45E-22	Pnpt1/Dnajc15/Cox6a2/Bckdk/Mrps28/Mrpl10/Hsd17b10/Mrpl44/Mrpl51/Mrps11/Mpv17l2/Mrps7/Mtx1/Timm10b/Mrpl2/Timm50/Mrpl52/Tomm70a/Mrpl4/Mrps24/Dmac1/Mrpl34/Mrps36/Ndufa11/Pam16/Mrps18a/Mrpl28/Mrpl12/Timm10/Pink1/Tomm7/Mrpl41/Mrps12/Ndufa6/Mrpl30/Chchd6/Ndufb11/Ndufb7/Mrps21/Ndufs8/Mrpl42/Ndufs7/Ndufs6/Smdt1/Ndufv3/Ndufa8/Ndufa13/Ndufb10/Sdhb/Atp5e/Ndufa3/Ndufa7/Atp5k/Cox5a/Ndufa2/Atp5g3/Atp5o/Ndufb8/Ndufa4/Atp5h/Chchd10/Uqcr10/Cox4i1/Cox6a1

GO	small ribosomal subunit	37/755	82/12262	1.41E-23	9.77E-22	8.89E-22	Gm6576/Gm5786/Mrps28/Gm9493/Rps20/Mrps11/Mrps7/Mrps24/Mrps36/Hba-a2/Hba-a1/Rack1/Mrps18a/Mrps12/Rps9/Rps18/Rps5/Rps27a/Rps24/Rps6/Rps3/Rps4x/Rpsa/Rps23/Rps10/Mrps21/Rps17/Mrpl42/Rps28/Rps13/Rps11/Rps3a1/Fau/Rps15/Uba52/Rps14/Rps27
GO	cytosolic small ribosomal subunit	28/755	51/12262	3.98E-21	2.45E-19	2.22E-19	Gm6576/Gm5786/Gm9493/Rps20/Hba-a2/Hba-a1/Rack1/Rps9/Rps18/Rps5/Rps27a/Rps24/Rps6/Rps3/Rps4x/Rpsa/Rps23/Rps10/Rps17/Rps28/Rps13/Rps11/Rps3a1/Fau/Rps15/Uba52/Rps14/Rps27
GO	structural molecule activity	82/733	416/11958	6.88E-22	2.42E-19	2.33E-19	Scara3/Gm6576/Nup35/Dag1/Npnt/Gm10036/Gm5786/Rpl7l1/Mrpl10/Rps20/Mrpl51/Mrps11/Mrps7/Gm10020/Gm10073/Mrpl2/Mrpl52/Rpl22/Mrpl4/Git1/Mrps24/Rpl28/Mrpl34/Rpl29/Rpl9-ps6/Rpl23a-ps3/Rpl15/Mrps18a/Mrpl28/Rpl10a/Mrpl12/Rpl18/Rpl35a/Mrpl41/Mrps12/Rps9/Rps18/Rps5/Rps27a/Rps24/Rplp2/Rpl14/Mrpl30/Rps6/Rpl6/Rps3/Rps4x/Rpsa/Rpl7/Rpl27a/Rps23/Rps10/Mrps21/Cope/Rpl36/Rpl30/Rps17/Rpl35/Rpl27/Rplp0/Rps28/Rpl31/Rpl39/Rps13/Rpl13/Rps11/Rpl8/Rps3a1/Fau/Rpl9/Rpl3/Rpl26/Rps15/Rpl13a/Rpl41/Rpl24/Rpl19/Rps14/Rpl4/Ndufa7/Rps27/Rplp1
GO	inner mitochondrial membrane protein complex	36/755	108/12262	9.82E-18	5.43E-16	4.94E-16	Dnajc15/Cox6a2/Timm10b/Timm50/Dmac1/Ndufa11/Pam16/Timm10/Ndufa6/Chchd6/Ndufb11/Ndufb7/Ndufs8/Ndufs7/Ndufs6/Smdt1/Ndufv3/Ndufa8/Ndufa13/Ndufb10/Sdhb/Atp5e/Ndufa3/Ndufa7/Atp5k/Cox5a/Ndufa2/Atp5g3/Atp5o/Ndufb8/Ndufa4/Atp5h/Chchd10/Uqcr10/Cox4i1/Cox6a1
Reactome	Formation of the ternary complex, and subsequently, the 43S complex	26/419	50/5985	1.13E-17	5.86E-16	5.23E-16	Eif3b/Rps20/Eif3f/Eif3g/Eif3h/Eif3i/Rps9/Rps18/Rps5/Rps27a/Rps24/Rps6/Rps3/Rps4x/Rpsa/Rps23/Rps10/Eif3k/Rps17/Rps28/Rps13/Rps11/Rps3a1/Rps15/Rps14/Rps27
GO	mitochondrial membrane part	47/755	187/12262	3.58E-17	1.80E-15	1.64E-15	Cox18/Mul1/Dnajc15/Cox6a2/Ptpmt1/Mtx1/Timm10b/Timm50/Tomm70a/Dmac1/Phb/Ndufa11/Pam16/Timm10/Pink1/Tomm7/Coa3/Ndufa6/Chchd6/Ndufb11/Ndufb7/Ndufs8/Ndufs7/Ndufs6/Smdt1/Ndufv3/Ndufa8/Ndufa13/Cisd1/Ndufb10/Sdhb/Atp5e/Ndufa3/Ndufa7/Atp5k/Cox5a/Ndufa2/Atp5g3/Atp5o/Ndufb8/Ndufa4/Cox7a2/Atp5h/Chchd10/Uqcr10/Cox4i1/Cox6a1
Reactome	Translation initiation complex formation	26/419	57/5985	7.19E-16	3.25E-14	2.90E-14	Eif3b/Rps20/Eif3f/Eif3g/Eif3h/Eif3i/Rps9/Rps18/Rps5/Rps27a/Rps24/Rps6/Rps3/Rps4x/Rpsa/Rps23/Rps10/Eif3k/Rps17/Rps28/Rps13/Rps11/Rps3a1/Rps15/Rps14/Rps27
Reactome	Ribosomal scanning and start codon recognition	26/419	57/5985	7.19E-16	3.25E-14	2.90E-14	Eif3b/Rps20/Eif3f/Eif3g/Eif3h/Eif3i/Rps9/Rps18/Rps5/Rps27a/Rps24/Rps6/Rps3/Rps4x/Rpsa/Rps23/Rps10/Eif3k/Rps17/Rps28/Rps13/Rps11/Rps3a1/Rps15/Rps14/Rps27
GO	mitochondrial inner membrane	66/755	363/12262	8.45E-16	3.89E-14	3.54E-14	Endog/Mrs2/Cox18/Dnajc15/Cox6a2/Hsd17b10/Mpv17l2/Ptpmt1/Mtx1/Timm10b/Timm50/Dnajc30/Tufm/Dhrs1/Phb2/Dmac1/Ociad2/Coq7/Phb/Mpv17/Ndufa11/Slc1a3/Pam16/Mtch1/Sirt3/Timm10/Pink1/Coa3/Ndufa6/Chchd6/Rps3/Ndufb11/Ndufb7/Mrps21/Ndufs8/Tmem256/Ndufs7/Ndufs6/Smdt1/Ndufv3/Higd2a/Ndufa8/Ndufa13/Ndufb10/Sdhb/Atp5e/Mdh2/Ndufa3/Ndufa7/Atp5k/Cox5a/Ndufa2/Atp5g3/Atp5o/Ndufb8/Ndufa4/Cox7a2/Atp5h/Timm8b/Chchd10/Uqcr10/Gpx4/Cox4i1/Cox6b1/Cox6a1/Cox8a
Reactome	Activation of the mRNA upon binding of the cap-binding complex and eIFs, and subsequent binding to 43S	26/419	58/5985	1.22E-15	5.19E-14	4.64E-14	Eif3b/Rps20/Eif3f/Eif3g/Eif3h/Eif3i/Rps9/Rps18/Rps5/Rps27a/Rps24/Rps6/Rps3/Rps4x/Rpsa/Rps23/Rps10/Eif3k/Rps17/Rps28/Rps13/Rps11/Rps3a1/Rps15/Rps14/Rps27
GO	respiratory chain complex	25/755	62/12262	6.17E-15	2.63E-13	2.39E-13	Cox6a2/Dmac1/Ndufa11/Ndufa6/Ndufb11/Ndufb7/Ndufs8/Ndufs7/Ndufs6/Ndufv3/Ndufa8/Ndufa13/Ndufb10/Sdhb/Ndufa3/Ndufa7/Cox5a/Ndufa2/Ndufb8/Ndufa4/Uqcr10/Cox4i1/Cox6b1/Cox6a1/Cox8a
GO	respiratory chain	26/755	68/12262	8.13E-15	3.21E-13	2.92E-13	Cox6a2/Dmac1/Ndufa11/Ndufa6/Ndufb11/Ndufb7/Ndufs8/Ndufs7/Ndufs6/Ndufv3/Ndufa8/Ndufa13/Ndufb10/Sdhb/Ndufa3/Ndufa7/Cox5a/Ndufa2/Ndufb8/Ndufa4/Cox7a2/Uqcr10/Cox4i1/Cox6b1/Cox6a1/Cox8a
GO	organelle inner membrane	66/755	393/12262	4.61E-14	1.70E-12	1.55E-12	Endog/Mrs2/Cox18/Dnajc15/Cox6a2/Hsd17b10/Mpv17l2/Ptpmt1/Mtx1/Timm10b/Timm50/Dnajc30/Tufm/Dhrs1/Phb2/Dmac1/Ociad2/Coq7/Phb/Mpv17/Ndufa11/Slc1a3/Pam16/Mtch1/Sirt3/Timm10/Pink1/Coa3/Ndufa6/Chchd6/Rps3/Ndufb11/Ndufb7/Mrps21/Ndufs8/Tmem256/Ndufs7/Ndufs6/Smdt1/Ndufv3/Higd2a/Ndufa8/Ndufa13/Ndufb10/Sdhb/Atp5e/Mdh2/Ndufa3/Ndufa7/Atp5k/Cox5a/Ndufa2/Atp5g3/Atp5o/Ndufb8/Ndufa4/Cox7a2/Atp5h/Timm8b/Chchd10/Uqcr10/Gpx4/Cox4i1/Cox6b1/Cox6a1/Cox8a
KEGG	Oxidative phosphorylation	33/334	95/4389	1.34E-14	1.69E-12	1.69E-12	Cox10/Cox6a2/Atp6v0e/Ndufa11/Ndufa6/Ndufb11/Ndufb7/Ndufs8/Ndufs7/Ndufs6/Ndufv3/Ndufa8/Ndufa13/Ndufb10/Atp6v1f/Sdhb/Atp5e/Ndufa3/Ndufa7/Atp5k/Cox5a/Ndufa2/Atp5g3/Atp5o/Ndufa4/Cox7a2/Atp6v0b/Atp5h/Uqcr10/Cox4i1/Cox6b1/Cox6a1/Cox8a
Reactome	Metabolism of RNA	79/419	478/5985	7.19E-14	2.89E-12	2.58E-12	Nop14/Nup35/Edc3/Rbm22/Ppie/Nxt1/Sf3b4/Nip7/Snrnp40/Sf3b5/Nob1/Gtf2h1/Lsm1/Emg1/Zmat5/Csnk1e/Paip1/Rps20/Imp3/Exosc4/Snrpd2/Rpl22/Rpl28/Lsm4/Lsm7/Hnrnpu/Snrnp25/Gemin7/Rpl29/Pcbp2/Polr2e/Rpl15/Rpl18/Rpl35a/Snrpb/Rpl36a/Rps9/Rps18/Rps5/Rps27a/Rps24/Rplp2/Rpl14/Rps6/Rpl6/Rps3/Rps4x/Rpsa/Rpl7/Rpl27a/Rps23/Rpl36al/Rps10/Rpl30/Rps17/Rpl35/Rpl27/Rplp0/Rps28/Rpl31/Rpl39/Rps13/Rpl13/Rps11/Rpl8/Rps3a1/Rpl9/Rpl3/Rpl26/Rps15/Rpl13a/Uba52/Rpl24/Rpl19/Rps14/Rpl4/Rps27/Rplp1/Ubb
GO	mitochondrial respiratory chain	24/755	63/12262	9.77E-14	3.38E-12	3.07E-12	Cox6a2/Dmac1/Ndufa11/Ndufa6/Ndufb11/Ndufb7/Ndufs8/Ndufs7/Ndufs6/Ndufv3/Ndufa8/Ndufa13/Ndufb10/Sdhb/Ndufa3/Ndufa7/Cox5a/Ndufa2/Ndufb8/Ndufa4/Cox7a2/Uqcr10/Cox4i1/Cox6a1
KEGG	Parkinson disease	33/334	103/4389	1.93E-13	1.62E-11	1.62E-11	Gnal/Cox6a2/Ube2g1/Ndufa11/Pink1/Ndufa6/Ndufb11/Ndufb7/Ndufs8/Ndufs7/Ndufs6/Ndufv3/Ndufa8/Ndufa13/Ndufb10/Sdhb/Atp5e/Ndufa3/Ndufa7/Cox5a/Ndufa2/Atp5g3/Atp5o/Uchl1/Ndufa4/Cox7a2/Atp5h/Uqcr10/Ubb/Cox4i1/Cox6b1/Cox6a1/Cox8a
Hallmark	OXIDATIVE_PHOSPHORYLATION	43/231	197/3242	4.64E-12	2.18E-10	2.15E-10	Cox10/Atp6v0e/Hsd17b10/Mrps11/Ech1/Timm50/Tomm70a/Phb2/Mrpl34/Timm10/Mrps12/Ndufa6/Ndufb7/Ndufs8/Ndufs7/Ndufs6/Mgst3/Ndufa8/Gpi1/Atp6v1f/Sdhb/Atp5e/Mdh2/Ndufa3/Ndufa7/Atp5k/Cox5a/Ndufa2/Atp5g3/Atp5o/Ndufb8/Ndufa4/Ldhb/Cox7a2/Atp6v0b/Atp5h/Timm8b/Uqcr10/Gpx4/Cox4i1/Cox6b1/Cox6a1/Cox8a
GO	polysomal ribosome	15/755	30/12262	3.94E-11	1.28E-09	1.16E-09	Pnpt1/Rpl29/Eif3h/Rpl10a/Rpl18/Btf3/Rpl6/Rps23/Rpl30/Rps28/Rpl31/Rpl39/Rpl8/Rpl24/Rpl19
GO	cytoplasmic translation	26/733	85/12053	2.57E-12	1.02E-08	1.02E-08	Cpeb4/Gm10020/Gm10073/Rpl29/Rpl9-ps6/Rpl15/Drg1/Rpl10a/Rpl18/Rpl35a/Rpl6/Rpsa/Rps23/Rpl36/Rpl30/Rplp0/Rps28/Rpl31/Rpl39/Rpl8/Rpl9/Rpl26/Rpl13a/Rpl24/Rpl19/Rplp1
GO	mitochondrial respiratory chain complex I	16/755	41/12262	8.80E-10	2.43E-08	2.21E-08	Dmac1/Ndufa11/Ndufa6/Ndufb11/Ndufb7/Ndufs8/Ndufs7/Ndufs6/Ndufv3/Ndufa8/Ndufa13/Ndufb10/Ndufa3/Ndufa7/Ndufa2/Ndufb8
GO	NADH dehydrogenase complex	16/755	41/12262	8.80E-10	2.43E-08	2.21E-08	Dmac1/Ndufa11/Ndufa6/Ndufb11/Ndufb7/Ndufs8/Ndufs7/Ndufs6/Ndufv3/Ndufa8/Ndufa13/Ndufb10/Ndufa3/Ndufa7/Ndufa2/Ndufb8
GO	respiratory chain complex I	16/755	41/12262	8.80E-10	2.43E-08	2.21E-08	Dmac1/Ndufa11/Ndufa6/Ndufb11/Ndufb7/Ndufs8/Ndufs7/Ndufs6/Ndufv3/Ndufa8/Ndufa13/Ndufb10/Ndufa3/Ndufa7/Ndufa2/Ndufb8
KEGG	Thermogenesis	37/334	164/4389	6.97E-10	4.29E-08	4.29E-08	Coa4/Cox18/Cox10/Cox6a2/Grb2/Adcy1/Ndufa11/Coa3/Ndufa6/Rps6/LOC105244208/Ndufb11/Ndufb7/Ndufs8/Ndufs7/Ndufs6/Cox14/Ndufv3/Ndufa8/Ndufa13/Ndufb10/Sdhb/Atp5e/Ndufa3/Ndufa7/Atp5k/Cox5a/Ndufa2/Atp5g3/Atp5o/Ndufa4/Cox7a2/Atp5h/Uqcr10/Cox4i1/Cox6b1/Cox6a1/Cox8a
KEGG	Alzheimer disease	32/334	129/4389	8.48E-10	4.29E-08	4.29E-08	Cox6a2/Gapdh/Gapdh-ps15/Hsd17b10/Psenen/Ndufa11/Cdk5/Ndufa6/Ndufb11/Ndufb7/Ndufs8/Ndufs7/Ndufs6/Ndufv3/Ndufa8/Ndufa13/Ndufb10/Sdhb/Atp5e/Ndufa3/Ndufa7/Cox5a/Ndufa2/Atp5g3/Atp5o/Ndufa4/Cox7a2/Atp5h/Uqcr10/Cox4i1/Cox6b1/Cox6a1/Cox8a
GO	rRNA binding	21/733	68/11958	3.14E-10	7.36E-08	7.08E-08	Emg1/Mrps11/Imp3/Mrps7/Mrps18a/Rps9/Rps18/Rps5/Rpl6/Rps3/Rps4x/Rpl7/Rplp0/Rps13/Rps11/Rpl8/Rpl9/Rpl3/Rpl19/Rps14/Rpl4
GO	polysome	20/755	69/12262	3.14E-09	8.26E-08	7.52E-08	Pnpt1/Rpl29/Drg1/Eif3h/Rpl10a/Rpl18/Btf3/Rps6/Rpl6/Rps3/Rps4x/Rpl7/Rps23/Rpl30/Rps28/Rpl31/Rpl39/Rpl8/Rpl24/Rpl19
KEGG	Non-alcoholic fatty liver disease (NAFLD)	27/334	106/4389	1.03E-08	4.33E-07	4.33E-07	Adipor2/Cox6a2/Adipor1/Xbp1/Ndufa11/Ndufa6/Ndufb11/Ndufb7/Ndufs8/Ndufs7/Ndufs6/Ndufv3/Ndufa8/Ndufa13/Ndufb10/Sdhb/Ndufa3/Ndufa7/Cox5a/Ndufa2/Ndufa4/Cox7a2/Uqcr10/Cox4i1/Cox6b1/Cox6a1/Cox8a
GO	organellar ribosome	22/755	92/12262	2.61E-08	6.27E-07	5.70E-07	Mrps28/Mrpl10/Mrpl44/Mrpl51/Mrps11/Mpv17l2/Mrps7/Mrpl2/Mrpl52/Mrpl4/Mrps24/Mrpl34/Mrps36/Mrps18a/Mrpl28/Mrpl12/Mrpl41/Mrps12/Mrpl30/Mrps21/Mrpl42/Ndufa7
GO	mitochondrial ribosome	22/755	92/12262	2.61E-08	6.27E-07	5.70E-07	Mrps28/Mrpl10/Mrpl44/Mrpl51/Mrps11/Mpv17l2/Mrps7/Mrpl2/Mrpl52/Mrpl4/Mrps24/Mrpl34/Mrps36/Mrps18a/Mrpl28/Mrpl12/Mrpl41/Mrps12/Mrpl30/Mrps21/Mrpl42/Ndufa7
KEGG	Huntington disease	32/334	144/4389	1.60E-08	5.77E-07	5.77E-07	Cox6a2/Polr2j/Ndufa11/Polr2e/Ndufa6/Ndufb11/Ndufb7/Ndufs8/Gpx1/Ap2s1/Ndufs7/Ndufs6/Ndufv3/Ndufa8/Ndufa13/Ndufb10/Sdhb/Atp5e/Ndufa3/Ndufa7/Cox5a/Ndufa2/Atp5g3/Atp5o/Ndufa4/Cox7a2/Atp5h/Uqcr10/Cox4i1/Cox6b1/Cox6a1/Cox8a
GO	mitochondrion organization	59/733	409/12053	3.81E-10	7.56E-07	7.56E-07	Coa4/Pnpt1/Cluh/Slc9a1/Tigar/Cox18/Mul1/Cox10/Dnajc15/Trak1/Dnlz/Bad/Hsd17b10/Triap1/Siva1/Timm50/Tomm70a/Phb2/Dmac1/Coq7/Ptpn5/Dctn6/Phb/Mpv17/Ndufa11/Pam16/Aip/Cdk5/Timm10/Pink1/Tomm7/Rnf7/Coa3/Gabarap/Ndufa6/Chchd6/Ndufb11/Map1lc3b/Ndufb7/Ndufs8/Gpx1/Ndufs7/Ndufs6/Cox14/Higd2a/Ndufa8/Ndufa13/Ndufb10/Ndufa3/Ndufa2/Ndufb8/Map1lc3a/Gabarapl1/Rab3a/Cox7a2/Chchd10/Uqcr10/Chchd2/Atpif1
GO	oxidoreductase complex	21/755	86/12262	3.65E-08	8.40E-07	7.65E-07	Cyba/Bckdk/Dmac1/Mrps36/Ndufa11/Ndufa6/Ndufb11/Ndufb7/Ndufs8/Ndufs7/Ndufs6/Ndufv3/Ndufa8/Ndufa13/Ndufb10/Sdhb/Ndufa3/Ndufa7/Ndufa2/Ndufb8/Uqcr10
GO	ribosome biogenesis	43/733	265/12053	2.84E-09	3.76E-06	3.76E-06	Riox2/Nop14/Pten/Gm10036/Nip7/Nob1/Drosha/Gm9493/Rpl7l1/Mrpl10/Ipo4/Emg1/Mrps11/Imp3/Exosc4/Mpv17l2/Mrps7/Nhp2/Eif6/Rpl23a-ps3/Eri3/Rpl10a/Rpl35a/Nop10/Rps5/Rps24/Rpl14/Rps6/Rpl6/Rpsa/Rpl7/Rps10/Rps17/Rpl35/Rpl27/Rplp0/Rps28/Rpl3/Rpl26/Rps15/Rpl24/Rps14/Rps27
Reactome	Respiratory electron transport, ATP synthesis by chemiosmotic coupling, and heat production by uncoupling proteins.	19/419	69/5985	1.34E-07	5.11E-06	4.56E-06	Ecsit/Ndufa6/Ndufb11/Ndufb7/Ndufs7/Ndufs6/Ndufv3/Ndufa8/Ndufa13/Ndufb10/Atp5e/Ndufa3/Ndufa7/Atp5k/Ndufa2/Atp5g3/Atp5o/Ndufb8/Atp5h

Reactome	The citric acid (TCA) cycle and respiratory electron transport	25/419	113/5985	1.61E-07	5.85E-06	5.22E-06	Me2/Gstz1/Ecsit/Ndufa6/Hagh/Ndufb11/Ndufb7/Ndufs7/Ndufs6/Ndufv3/Ndufa8/Ndufa13/Ndufb10/Sdhb/Atp5e/Mdh2/Ndufa3/Ndufa7/Atp5k/Ndufa2/Atp5g3/Atp5o/Ndufb8/Ldhb/Atp5h
GO	respiratory chain complex IV	7/755	10/12262	3.33E-07	7.36E-06	6.70E-06	Cox6a2/Cox5a/Ndufa4/Cox4i1/Cox6b1/Cox6a1/Cox8a
Reactome	Mitochondrial translation termination	21/419	85/5985	2.24E-07	7.73E-06	6.90E-06	Mrrf/Mrps28/Mrpl10/Mrpl44/Mrpl51/Mrps7/Mrpl2/Mrpl52/Mrpl4/Mrps24/Mrpl34/Mrps36/Mrps18a/Mrpl28/Mrps33/Mrpl12/Mrpl41/Mrps12/Mrpl30/Mrps21/Mrpl42
Reactome	Mitochondrial translation	21/419	86/5985	2.78E-07	9.14E-06	8.16E-06	Mrrf/Mrps28/Mrpl10/Mrpl44/Mrpl51/Mrps7/Mrpl2/Mrpl52/Mrpl4/Mrps24/Mrpl34/Mrps36/Mrps18a/Mrpl28/Mrps33/Mrpl12/Mrpl41/Mrps12/Mrpl30/Mrps21/Mrpl42
GO	cytochrome complex	9/755	19/12262	6.40E-07	1.36E-05	1.24E-05	Cox10/Cox6a2/Cox5a/Ndufa4/Uqcr10/Cox4i1/Cox6b1/Cox6a1/Cox8a
Reactome	Mitochondrial translation elongation	20/419	83/5985	6.75E-07	2.13E-05	1.90E-05	Mrps28/Mrpl10/Mrpl44/Mrpl51/Mrps7/Mrpl2/Mrpl52/Mrpl4/Mrps24/Mrpl34/Mrps36/Mrps18a/Mrpl28/Mrps33/Mrpl12/Mrpl41/Mrps12/Mrpl30/Mrps21/Mrpl42
GO	mitochondrial matrix	35/755	241/12262	1.76E-06	3.61E-05	3.29E-05	Ptcd1/Mpg/Glrx5/Dnajc15/Bckdk/Mrps28/Mrpl10/Hsd17b10/Mrpl44/Mrpl51/Mrps11/Mpv17l2/Mrps7/Mrpl2/Mrpl52/Tufm/Clpp/Mrpl4/Mrps24/Mrpl34/Mrps36/Pam16/Mrps18a/Mrpl28/Mrpl12/Sirt3/Mrpl41/Mrps12/Hagh/Mrpl30/Rps3/Mrps21/Mrpl42/Mdh2/Ndufa7
Reactome	Complex I biogenesis	14/419	45/5985	1.22E-06	3.69E-05	3.29E-05	Ecsit/Ndufa6/Ndufb11/Ndufb7/Ndufs7/Ndufs6/Ndufv3/Ndufa8/Ndufa13/Ndufb10/Ndufa3/Ndufa7/Ndufa2/Ndufb8
GO	ribosome assembly	18/733	65/12053	3.50E-08	3.48E-05	3.48E-05	Gm10036/Nip7/Mrps11/Mpv17l2/Mrps7/Eif6/Rpl23a-ps3/Rps5/Rpl6/Rpsa/Rps10/Rplp0/Rps28/Rpl3/Rps15/Rpl24/Rps14/Rps27
GO	proton transmembrane transporter activity	18/733	76/11958	5.24E-07	8.44E-05	8.12E-05	Slc9a1/Cox10/Cox6a2/Atp6v0e/Atp6v1g2/Atp6v1f/Atp5e/Atp5k/Cox5a/Atp5g3/Atp5o/Ndufa4/Cox7a2/Atp6v0b/Atp5h/Cox4i1/Cox6a1/Cox8a
GO	cytochrome-c oxidase activity	8/733	15/11958	8.40E-07	8.44E-05	8.12E-05	Cox10/Cox6a2/Cox5a/Ndufa4/Cox7a2/Cox4i1/Cox6a1/Cox8a
GO	heme-copper terminal oxidase activity	8/733	15/11958	8.40E-07	8.44E-05	8.12E-05	Cox10/Cox6a2/Cox5a/Ndufa4/Cox7a2/Cox4i1/Cox6a1/Cox8a
GO	oxidoreductase activity, acting on a heme group of donors, oxygen as acceptor	8/733	15/11958	8.40E-07	8.44E-05	8.12E-05	Cox10/Cox6a2/Cox5a/Ndufa4/Cox7a2/Cox4i1/Cox6a1/Cox8a
GO	ribonucleoprotein complex biogenesis	52/733	399/12053	1.35E-07	0.000107419	0.000107419	Riox2/Nop14/Edc3/Pten/Gm10036/Nip7/Nob1/Ruvbl2/Drosha/Gm9493/Rpl7l1/Mrpl10/Ipo4/Emg1/Mrps11/Zrsr2/Imp3/Exosc4/Mpv17l2/Snrpd2/Mrps7/Nhp2/Eif6/Lsm4/Gemin7/Rpl23a-ps3/Eri3/Rpl10a/Rpl35a/Nop10/Snrpb/Rps5/Rps24/Rpl14/Rps6/Rpl6/Rpsa/Rpl7/Rps23/Rps10/Rps17/Rpl35/Rpl27/Rplp0/Rps28/Rpl3/Rpl26/Rps15/Rpl13a/Rpl24/Rps14/Rps27
Reactome	Respiratory electron transport	14/419	50/5985	4.97E-06	0.000143897	0.000128457	Ecsit/Ndufa6/Ndufb11/Ndufb7/Ndufs7/Ndufs6/Ndufv3/Ndufa8/Ndufa13/Ndufb10/Ndufa3/Ndufa7/Ndufa2/Ndufb8
GO	oxidoreductase activity, acting on a heme group of donors	8/733	16/11958	1.59E-06	0.000139708	0.00013451	Cox10/Cox6a2/Cox5a/Ndufa4/Cox7a2/Cox4i1/Cox6a1/Cox8a
GO	purine ribonucleoside triphosphate metabolic process	34/733	216/12053	2.78E-07	0.000172633	0.000172633	Tigar/Dnajc15/Cox6a2/Bad/Dnajc30/Mocs2/Eif6/Coq7/Mpi/Itpa/Ak1/Pink1/Nme1/Ndufs8/Guk1/Ndufs6/Ndufv3/Ndufa8/Gpi1/Atp5e/Ndufa7/Atp5k/Cox5a/Atp5g3/Atp5o/Tpi1/Ndufb8/Cox7a2/Atp5h/Chchd10/Uqcr10/Cox4i1/Cox6a1/Atpif1
GO	mitochondrial respiratory chain complex assembly	18/733	74/12053	3.04E-07	0.000172633	0.000172633	Coa4/Cox18/Dmac1/Ndufa11/Coa3/Ndufa6/Ndufb11/Ndufb7/Ndufs8/Ndufs7/Cox14/Ndufa8/Ndufa13/Ndufb10/Ndufa3/Ndufa2/Ndufb8/Uqcr10
GO	ribonucleoside triphosphate metabolic process	34/733	220/12053	4.33E-07	0.000192576	0.000192576	Tigar/Dnajc15/Cox6a2/Bad/Dnajc30/Mocs2/Eif6/Coq7/Mpi/Itpa/Ak1/Pink1/Nme1/Ndufs8/Guk1/Ndufs6/Ndufv3/Ndufa8/Gpi1/Atp5e/Ndufa7/Atp5k/Cox5a/Atp5g3/Atp5o/Tpi1/Ndufb8/Cox7a2/Atp5h/Chchd10/Uqcr10/Cox4i1/Cox6a1/Atpif1
GO	oxidative phosphorylation	18/733	76/12053	4.67E-07	0.000192576	0.000192576	Dnajc15/Cox6a2/Dnajc30/Coq7/Pink1/Ndufs8/Ndufs6/Ndufv3/Ndufa8/Ndufa7/Cox5a/Atp5o/Ndufb8/Cox7a2/Chchd10/Uqcr10/Cox4i1/Cox6a1
GO	ATP metabolic process	31/733	192/12053	5.28E-07	0.000192576	0.000192576	Tigar/Dnajc15/Cox6a2/Bad/Dnajc30/Eif6/Coq7/Mpi/Ak1/Pink1/Ndufs8/Guk1/Ndufs6/Ndufv3/Ndufa8/Gpi1/Atp5e/Ndufa7/Atp5k/Cox5a/Atp5g3/Atp5o/Tpi1/Ndufb8/Cox7a2/Atp5h/Chchd10/Uqcr10/Cox4i1/Cox6a1/Atpif1
GO	purine nucleoside triphosphate metabolic process	34/733	222/12053	5.38E-07	0.000192576	0.000192576	Tigar/Dnajc15/Cox6a2/Bad/Dnajc30/Mocs2/Eif6/Coq7/Mpi/Itpa/Ak1/Pink1/Nme1/Ndufs8/Guk1/Ndufs6/Ndufv3/Ndufa8/Gpi1/Atp5e/Ndufa7/Atp5k/Cox5a/Atp5g3/Atp5o/Tpi1/Ndufb8/Cox7a2/Atp5h/Chchd10/Uqcr10/Cox4i1/Cox6a1/Atpif1
GO	mitochondrial ATP synthesis coupled electron transport	14/733	48/12053	5.82E-07	0.000192576	0.000192576	Dnajc15/Cox6a2/Coq7/Pink1/Ndufs8/Ndufs6/Ndufv3/Ndufa8/Ndufa7/Cox5a/Ndufb8/Uqcr10/Cox4i1/Cox6a1
GO	organellar large ribosomal subunit	14/755	60/12262	1.22E-05	0.000232415	0.000211467	Mrpl10/Mrpl44/Mrpl51/Mpv17l2/Mrpl2/Mrpl52/Mrpl4/Mrpl34/Mrps18a/Mrpl28/Mrpl12/Mrpl41/Mrpl30/Mrpl42
GO	mitochondrial large ribosomal subunit	14/755	60/12262	1.22E-05	0.000232415	0.000211467	Mrpl10/Mrpl44/Mrpl51/Mpv17l2/Mrpl2/Mrpl52/Mrpl4/Mrpl34/Mrps18a/Mrpl28/Mrpl12/Mrpl41/Mrpl30/Mrpl42
GO	ATP synthesis coupled electron transport	14/733	49/12053	7.69E-07	0.000235099	0.000235099	Dnajc15/Cox6a2/Coq7/Pink1/Ndufs8/Ndufs6/Ndufv3/Ndufa8/Ndufa7/Cox5a/Ndufb8/Uqcr10/Cox4i1/Cox6a1
GO	NADH dehydrogenase complex assembly	13/733	43/12053	9.33E-07	0.000246193	0.000246193	Dmac1/Ndufa11/Ndufa6/Ndufb11/Ndufb7/Ndufs8/Ndufs7/Ndufa8/Ndufa13/Ndufb10/Ndufa3/Ndufa2/Ndufb8
GO	mitochondrial respiratory chain complex I assembly	13/733	43/12053	9.33E-07	0.000246193	0.000246193	Dmac1/Ndufa11/Ndufa6/Ndufb11/Ndufb7/Ndufs8/Ndufs7/Ndufa8/Ndufa13/Ndufb10/Ndufa3/Ndufa2/Ndufb8
GO	ribosomal small subunit assembly	9/733	20/12053	9.91E-07	0.000246193	0.000246193	Mrps11/Mrps7/Rps5/Rpsa/Rps10/Rps28/Rps15/Rps14/Rps27
GO	respiratory electron transport chain	16/733	67/12053	1.80E-06	0.000420151	0.000420151	Dnajc15/Cox6a2/Coq7/Slc1a3/Pink1/Ndufs8/Ndufs6/Ndufv3/Ndufa8/Sdhb/Ndufa7/Cox5a/Ndufb8/Uqcr10/Cox4i1/Cox6a1
GO	oxidoreductase activity	56/733	496/11958	6.05E-06	0.000472399	0.000454821	Riox2/Me2/Cyp20a1/Gfod1/Pcbd2/Jmjd6/Cyba/Glrx5/Blvrb/Cox10/Ethe1/Tsta3/Cox6a2/Hbb-bt/Msrb2/Hsd17b10/Spr/Msra/Ecsit/Vkorc1/Kcnab2/Alkbh6/Dhrs1/Txndc17/Coq7/Hbb-bs/Mrps36/Hba-a2/Hba-a1/Crym/Txn2/Ndufb7/Ndufs8/Gpx1/Ndufs7/Mgst3/Ndufa13/Ftl1/Sdhb/Mdh2/Sh3bgrl3/Ndufa7/Cox5a/Ndufa2/Ndufb8/Akr1a1/Ndufa4/Ldhb/Cox7a2/Uqcr10/Gpx4/Cox4i1/Selenow/Cox6a1/Cox8a/Fth1
GO	nucleoside triphosphate metabolic process	34/733	237/12053	2.48E-06	0.000546762	0.000546762	Tigar/Dnajc15/Cox6a2/Bad/Dnajc30/Mocs2/Eif6/Coq7/Mpi/Itpa/Ak1/Pink1/Nme1/Ndufs8/Guk1/Ndufs6/Ndufv3/Ndufa8/Gpi1/Atp5e/Ndufa7/Atp5k/Cox5a/Atp5g3/Atp5o/Tpi1/Ndufb8/Cox7a2/Atp5h/Chchd10/Uqcr10/Cox4i1/Cox6a1/Atpif1
GO	electron transport chain	16/733	70/12053	3.34E-06	0.000698845	0.000698845	Dnajc15/Cox6a2/Coq7/Slc1a3/Pink1/Ndufs8/Ndufs6/Ndufv3/Ndufa8/Sdhb/Ndufa7/Cox5a/Ndufb8/Uqcr10/Cox4i1/Cox6a1
GO	electron transfer activity	13/733	52/11958	1.06E-05	0.000745062	0.000717339	Cyba/Glrx5/Cox10/Cox6a2/Sdhb/Sh3bgrl3/Cox5a/Ndufa4/Cox7a2/Uqcr10/Cox4i1/Cox6a1/Cox8a
GO	organellar small ribosomal subunit	9/755	30/12262	5.36E-05	0.000956784	0.000870549	Mrps28/Mrps11/Mrps7/Mrps24/Mrps36/Mrps18a/Mrps12/Mrps21/Mrpl42
GO	mitochondrial small ribosomal subunit	9/755	30/12262	5.36E-05	0.000956784	0.000870549	Mrps28/Mrps11/Mrps7/Mrps24/Mrps36/Mrps18a/Mrps12/Mrps21/Mrpl42
GO	nucleoside monophosphate metabolic process	32/733	224/12053	5.34E-06	0.001060917	0.001060917	Tigar/Dnajc15/Cox6a2/Bad/Dnajc30/Eif6/Coq7/Mpi/Nt5m/Ak1/Pink1/Ndufs8/Guk1/Ndufs6/Ndufv3/Ndufa8/Gpi1/Atp5e/Ndufa7/Atp5k/Cox5a/Atp5g3/Atp5o/Tpi1/Ndufb8/Cox7a2/Atp5h/Chchd10/Uqcr10/Cox4i1/Cox6a1/Atpif1
GO	purine nucleoside monophosphate metabolic process	31/733	215/12053	6.16E-06	0.001113034	0.001113034	Tigar/Dnajc15/Cox6a2/Bad/Dnajc30/Eif6/Coq7/Mpi/Ak1/Pink1/Ndufs8/Guk1/Ndufs6/Ndufv3/Ndufa8/Gpi1/Atp5e/Ndufa7/Atp5k/Cox5a/Atp5g3/Atp5o/Tpi1/Ndufb8/Cox7a2/Atp5h/Chchd10/Uqcr10/Cox4i1/Cox6a1/Atpif1
GO	purine ribonucleoside monophosphate metabolic process	31/733	215/12053	6.16E-06	0.001113034	0.001113034	Tigar/Dnajc15/Cox6a2/Bad/Dnajc30/Eif6/Coq7/Mpi/Ak1/Pink1/Ndufs8/Guk1/Ndufs6/Ndufv3/Ndufa8/Gpi1/Atp5e/Ndufa7/Atp5k/Cox5a/Atp5g3/Atp5o/Tpi1/Ndufb8/Cox7a2/Atp5h/Chchd10/Uqcr10/Cox4i1/Cox6a1/Atpif1
Reactome	Pink/Parkin Mediated Mitophagy	8/419	21/5985	4.88E-05	0.001357672	0.001211996	Tomm70a/Pink1/Tomm7/Rps27a/Map1lc3b/Uba52/Map1lc3a/Ubb
GO	ribonucleoside monophosphate metabolic process	31/733	218/12053	8.22E-06	0.001419965	0.001419965	Tigar/Dnajc15/Cox6a2/Bad/Dnajc30/Eif6/Coq7/Mpi/Ak1/Pink1/Ndufs8/Guk1/Ndufs6/Ndufv3/Ndufa8/Gpi1/Atp5e/Ndufa7/Atp5k/Cox5a/Atp5g3/Atp5o/Tpi1/Ndufb8/Cox7a2/Atp5h/Chchd10/Uqcr10/Cox4i1/Cox6a1/Atpif1
GO	U12-type spliceosomal complex	8/755	26/12262	0.000115018	0.001987652	0.001808504	Sf3b4/Sf3b5/Zmat5/Zrsr2/Snrpd2/Lsm7/Snrnp25/Snrpb
Hallmark	MYC_TARGETS_V1	29/231	196/3242	8.76E-05	0.002059519	0.002029537	Ruvbl2/Eif3b/Hddc2/Kars/Snrpd2/Tomm70a/Rpl22/Tufm/Nhp2/Phb2/Hdgf/Lsm7/Phb/Hnrnpu/Rack1/Rpl18/Tcp1/Rps5/Rpl14/Rps6/Psmb2/Rpl6/Rps3/Nme1/Rps10/Rplp0/Psmb3/Cox5a/Ppia
GO	generation of precursor metabolites and energy	37/733	291/12053	1.56E-05	0.002418903	0.002418903	Stk40/Pnpt1/Pygm/Tigar/Cox10/Dnajc15/Cox6a2/Dnajc30/Phb2/Ppp1cb/Eif6/Coq7/Mpi/Slc1a3/Sirt3/Pink1/Ndufs8/Ndufs7/Ndufs6/Ndufv3/Ndufa8/Gpi1/Cisd1/Ppp1ca/Sdhb/Mdh2/Ndufa7/Cox5a/Atp5o/Tpi1/Ndufb8/Gnas/Cox7a2/Chchd10/Uqcr10/Cox4i1/Cox6
GO	nucleotide metabolic process	49/733	431/12053	1.58E-05	0.002418903	0.002418903	Me2/Tigar/Mvk/Dcakd/Dnajc15/Cox6a2/Pgls/Bad/Kars/Adcy1/Kcnab2/Mcee/Dnajc30/Mocs2/Nt5c/Taldo1/Eif6/Coq7/Mpi/Nt5m/Itpa/Ak1/Pink1/Nme1/Ndufs8/Guk1/Ndufs6/Ndufv3/Ndufa8/Acot7/Gpi1/Atp5e/Mdh2/Ndufa7/Atp5k/Cox5a/Atp5g3/Hint1/Atp5o/Tpi1/Ndufb8/Ldhb/Cox7a2/Atp5h/Chchd10/Uqcr10/Cox4i1/Cox6a1/Atpif1
GO	ribosomal small subunit biogenesis	14/733	62/12053	1.58E-05	0.002418903	0.002418903	Nob1/Gm9493/Mrps11/Mrps7/Rps5/Rps24/Rps6/Rpsa/Rps10/Rps17/Rps28/Rps15/Rps14/Rps27
GO	eukaryotic translation initiation factor 3 complex	6/755	15/12262	0.000165294	0.002769921	0.002520267	Eif3b/Eif3f/Eif3g/Eif3h/Eif3i/Eif3k
Reactome	PTEN Regulation	13/419	57/5985	0.000114889	0.003080729	0.002750171	Phc1/Pten/Rragc/Chd3/Maf1/Lamtor1/Rps27a/Csnk2b/Lamtor2/Stub1/Lamtor5/Uba52/Ubb
Reactome	Macroautophagy	16/419	81/5985	0.000121763	0.003148452	0.002810628	Rragc/Tomm70a/Atg101/Pink1/Tomm7/Lamtor1/Dynll1/Gabarap/Rps27a/Lamtor2/Map1lc3b/Lamtor5/Uba52/Map1lc3a/Gabarapl1/Ubb
GO	NADH dehydrogenase (ubiquinone) activity	7/733	18/11958	5.54E-05	0.003024821	0.002912271	Ndufb7/Ndufs8/Ndufs7/Ndufa13/Ndufa7/Ndufa2/Ndufb8
GO	NADH dehydrogenase (quinone) activity	7/733	18/11958	5.54E-05	0.003024821	0.002912271	Ndufb7/Ndufs8/Ndufs7/Ndufa13/Ndufa7/Ndufa2/Ndufb8
GO	ribonucleoprotein complex binding	21/733	133/11958	5.59E-05	0.003024821	0.002912271	Cpeb4/Mrrf/Gtpbp6/Srp68/Snrpd2/Gm10073/Timm50/Eif6/Hnrnpu/Rack1/Rpl35a/Snrpb/Eif1b/Csnk2b/Rpsa/Nme1/Eif3k/Rpl35/Ppp1ca/Eif5a/Rplp1

GO	cellular respiration	22/733	135/12053	2.01E-05	0.002917697	0.002917697	Pnpt1/Cox10/Dnajc15/Cox6a2/Coq7/Slc1a3/Sirt3/Pink1/Ndufs8/Ndufs7/Ndufs6/Ndufv3/Ndufa8/Cisd1/Sdhb/Mdh2/Ndufa7/Cox5a/Ndufb8/Uqcr10/Cox4i1/Cox6a1
GO	nucleobase-containing small molecule metabolic process	53/733	484/12053	2.06E-05	0.002917697	0.002917697	Me2/Tigar/Mvk/Dcakd/Macrod2/Dnajc15/Tsta3/Cox6a2/Pgls/Bad/Kars/Adcy1/Kcnab2/Mcee/Dnajc30/Mocs2/Nt5c/Taldo1/Eif6/Ahcyl1/Cmas/Coq7/Mpi/Nt5m/Itpa/Ak1/Pink1/Nme1/Ndufs8/Guk1/Ndufs6/Ndufv3/Ndufa8/Acot7/Gpi1/Atp5e/Mdh2/Ndufa7/Atp5k/Cox5a/Atp5g3/Hint1/Atp5o/Tpi1/Ndufb8/Ldhb/Cox7a2/Atp5h/Chchd10/Uqcr10/Cox4i1/Cox6a1/Atpif1
GO	purine ribonucleotide metabolic process	40/733	330/12053	2.22E-05	0.002946841	0.002946841	Tigar/Mvk/Dcakd/Dnajc15/Cox6a2/Bad/Adcy1/Mcee/Dnajc30/Mocs2/Eif6/Coq7/Mpi/Itpa/Ak1/Pink1/Nme1/Ndufs8/Guk1/Ndufs6/Ndufv3/Ndufa8/Acot7/Gpi1/Atp5e/Ndufa7/Atp5k/Cox5a/Atp5g3/Hint1/Atp5o/Tpi1/Ndufb8/Cox7a2/Atp5h/Chchd10/Uqcr10/Cox4i1/Cox6a1/Atpif1
GO	ribosomal large subunit biogenesis	15/733	72/12053	2.22E-05	0.002946841	0.002946841	Gm10036/Nip7/Rpl7l1/Nhp2/Rpl23a-ps3/Rpl10a/Rpl35a/Rpl14/Rpl6/Rpl7/Rpl35/Rplp0/Rpl3/Rpl26/Rpl24
GO	ribose phosphate metabolic process	42/733	354/12053	2.34E-05	0.002995096	0.002995096	Tigar/Mvk/Dcakd/Dnajc15/Cox6a2/Pgls/Bad/Adcy1/Mcee/Dnajc30/Mocs2/Taldo1/Eif6/Coq7/Mpi/Itpa/Ak1/Pink1/Nme1/Ndufs8/Guk1/Ndufs6/Ndufv3/Ndufa8/Acot7/Gpi1/Atp5e/Ndufa7/Atp5k/Cox5a/Atp5g3/Hint1/Atp5o/Tpi1/Ndufb8/Cox7a2/Atp5h/Chchd10/Uqcr10/Cox4i1/Cox6a1/Atpif1
GO	nucleoside phosphate metabolic process	49/733	438/12053	2.42E-05	0.003005678	0.003005678	Me2/Tigar/Mvk/Dcakd/Dnajc15/Cox6a2/Pgls/Bad/Kars/Adcy1/Kcnab2/Mcee/Dnajc30/Mocs2/Nt5c/Taldo1/Eif6/Coq7/Mpi/Nt5m/Itpa/Ak1/Pink1/Nme1/Ndufs8/Guk1/Ndufs6/Ndufv3/Ndufa8/Acot7/Gpi1/Atp5e/Mdh2/Ndufa7/Atp5k/Cox5a/Atp5g3/Hint1/Atp5o/Tpi1/Ndufb8/Ldhb/Cox7a2/Atp5h/Chchd10/Uqcr10/Cox4i1/Cox6a1/Atpif1
GO	mitochondrial transport	24/733	158/12053	2.86E-05	0.003443864	0.003443864	Pnpt1/Mrs2/Slc9a1/Mul1/Dnajc15/Dnlz/Bad/Siva1/Timm50/Tomm70a/Dnajc30/Ptpn5/Slc1a3/Pam16/Aip/Crym/Timm10/Pink1/Tomm7/Smdt1/Ndufa13/Atp5o/Chchd10/Atpif1
GO	drug metabolic process	50/733	457/12053	3.61E-05	0.004220129	0.004220129	Abcd4/Sult1a1/Pcbd2/Cyba/Tigar/Ass1/Ethe1/Gstz1/Dnajc15/Cox6a2/Hbb-bt/Bad/Spr/Vkorc1/Dnajc30/Esd/Eif6/Ahcyl1/Coq7/Mpi/Hba-a1/Comt/Ak1/Pink1/Dynll1/Ndufs8/Gpx1/Guk1/Ndufs6/Ndufv3/Ndufa8/Gpi1/Sdhb/Atp5e/Mdh2/Ndufa7/Atp5k/Cox5a/Atp5g3/Atp5o/Tpi1/Ndufb8/Akr1a1/Cox7a2/Atp5h/Chchd10/Uqcr10/Cox4i1/Cox6a1/Atpif1
Reactome	Mitophagy	8/419	25/5985	0.000201917	0.005040954	0.004500067	Tomm70a/Pink1/Tomm7/Rps27a/Map1lc3b/Uba52/Map1lc3a/Ubb
GO	proton-transporting two-sector ATPase complex	9/755	37/12262	0.000316121	0.005141616	0.0046782	Atp6v0e/Atp6v1g2/Atp6v1f/Atp5e/Atp5k/Atp5g3/Atp5o/Atp6v0b/Atp5h
GO	ribonucleotide metabolic process	40/733	339/12053	4.13E-05	0.004691429	0.004691429	Tigar/Mvk/Dcakd/Dnajc15/Cox6a2/Bad/Adcy1/Mcee/Dnajc30/Mocs2/Eif6/Coq7/Mpi/Itpa/Ak1/Pink1/Nme1/Ndufs8/Guk1/Ndufs6/Ndufv3/Ndufa8/Acot7/Gpi1/Atp5e/Ndufa7/Atp5k/Cox5a/Atp5g3/Hint1/Atp5o/Tpi1/Ndufb8/Cox7a2/Atp5h/Chchd10/Uqcr10/Cox4i1/Cox6a1/Atpif1
GO	energy derivation by oxidation of organic compounds	28/733	205/12053	4.69E-05	0.005174159	0.005174159	Stk40/Pnpt1/Pygm/Tigar/Cox10/Dnajc15/Cox6a2/Ppp1cb/Coq7/Slc1a3/Sirt3/Pink1/Ndufs8/Ndufs7/Ndufs6/Ndufv3/Ndufa8/Cisd1/Ppp1ca/Sdhb/Mdh2/Ndufa7/Cox5a/Ndufb8/Gnas/Uqcr10/Cox4i1/Cox6a1
GO	NADH dehydrogenase activity	7/733	20/11958	0.000121077	0.006079784	0.005853561	Ndufb7/Ndufs8/Ndufs7/Ndufa13/Ndufa7/Ndufa2/Ndufb8
GO	purine-containing compound metabolic process	42/733	368/12053	5.82E-05	0.006253363	0.006253363	Tigar/Mvk/Dcakd/Macrod2/Dnajc15/Cox6a2/Bad/Adcy1/Mcee/Dnajc30/Mocs2/Eif6/Ahcyl1/Coq7/Mpi/Itpa/Ak1/Pink1/Nme1/Ndufs8/Guk1/Ndufs6/Ndufv3/Ndufa8/Acot7/Gpi1/Atp5e/Ndufa7/Atp5k/Cox5a/Atp5g3/Hint1/Atp5o/Tpi1/Ndufb8/Cox7a2/Atp5h/Chchd10/Uqcr10/Cox4i1/Cox6a1/Atpif1
GO	COP9 signalosome	8/755	31/12262	0.00044138	0.006973807	0.006345255	Plcg1/Cops8/Grb2/Gps1/Flot1/Dynll1/Cops6/Cops9
GO	purine nucleotide metabolic process	40/733	346/12053	6.55E-05	0.006845571	0.006845571	Tigar/Mvk/Dcakd/Dnajc15/Cox6a2/Bad/Adcy1/Mcee/Dnajc30/Mocs2/Eif6/Coq7/Mpi/Itpa/Ak1/Pink1/Nme1/Ndufs8/Guk1/Ndufs6/Ndufv3/Ndufa8/Acot7/Gpi1/Atp5e/Ndufa7/Atp5k/Cox5a/Atp5g3/Hint1/Atp5o/Tpi1/Ndufb8/Cox7a2/Atp5h/Chchd10/Uqcr10/Cox4i1/Cox6a1/Atpif1
GO	mitochondrial electron transport, NADH to ubiquinone	7/733	19/12053	7.90E-05	0.008050559	0.008050559	Dnajc15/Pink1/Ndufs8/Ndufs6/Ndufa8/Ndufa7/Ndufb8
GO	mitochondrial intermembrane space	12/755	66/12262	0.000616587	0.009471464	0.008617797	Coa4/Pnpt1/Triap1/Timm10b/Arl2/Timm10/Pink1/Ndufb7/Ndufa8/Timm8b/Chchd10/Chchd2
GO	proton-transporting two-sector ATPase complex, proton-transporting domain	6/755	19/12262	0.000724463	0.010827779	0.009851868	Atp6v0e/Atp5k/Atp5g3/Atp5o/Atp6v0b/Atp5h
GO	proton transmembrane transport	13/733	64/12053	0.000102362	0.010169622	0.010169622	Slc9a1/Atp6v0e/Dnajc30/Phb2/Ndufs7/Atp6v1f/Atp5e/Atp5k/Atp5g3/Atp5o/Atp6v0b/Atp5h/Chchd10
GO	ribonucleoprotein complex subunit organization	28/733	216/12053	0.00011869	0.011178115	0.011178115	Edc3/Mrrf/Gm10036/Nip7/Ruvbl2/Mrps11/Zrsr2/Mpv17l2/Snrpd2/Mrps7/Eif6/Lsm4/Gemin7/Rpl23a-ps3/Snrpb/Rps5/Rpl6/Rpsa/Rps23/Rps10/Rplp0/Rps28/Rpl3/Rps15/Rpl13a/Rpl24/Rps14/Rps27
GO	ribonucleoprotein complex assembly	27/733	205/12053	0.000119334	0.011178115	0.011178115	Edc3/Gm10036/Nip7/Ruvbl2/Mrps11/Zrsr2/Mpv17l2/Snrpd2/Mrps7/Eif6/Lsm4/Gemin7/Rpl23a-ps3/Snrpb/Rps5/Rpl6/Rpsa/Rps23/Rps10/Rplp0/Rps28/Rpl3/Rps15/Rpl13a/Rpl24/Rps14/Rps27
GO	mitochondrial transmembrane transport	13/733	65/12053	0.000120951	0.011178115	0.011178115	Pnpt1/Mrs2/Dnajc15/Dnlz/Timm50/Dnajc30/Slc1a3/Pam16/Timm10/Tomm7/Smdt1/Ndufa13/Atp5o
GO	mitochondrial gene expression	17/733	102/12053	0.000129558	0.011701486	0.011701486	Pnpt1/Hsd17b10/Mrpl44/Mrpl51/Mrps11/Mpv17l2/Mrpl2/Mrpl52/Tufm/Mrps18a/Mrpl12/Sirt3/Mrps12/Coa3/Mrps21/Ndufa7/Chchd10
GO	cofactor metabolic process	41/733	370/12053	0.000137007	0.012099218	0.012099218	Abcd4/Me2/Pcbd2/Cyba/Tigar/Mvk/Dcakd/Blvrb/Cox10/Ethe1/Gstz1/Alad/Pgls/Hebp1/Hbb-bt/Gsta4/Spr/Nubp2/Kcnab2/Mcee/Mocs2/Taldo1/Eif6/Ahcyl1/Coq7/Mpi/Mrps36/Hba-a1/Pink1/Hagh/Gpx1/Gstm5/Got1/Acot7/Gpi1/Mdh2/Tpi1/Akr1a1/Ldhb/Gpx4/Atpif1
GO	small ribosomal subunit rRNA binding	5/733	11/11958	0.000289123	0.013550214	0.013046025	Mrps11/Mrps18a/Rps3/Rps13/Rps14
GO	rRNA processing	24/733	177/12053	0.000179281	0.015488335	0.015488335	Nop14/Nob1/Gm9493/Rpl7l1/Emg1/Mrps11/Imp3/Exosc4/Nhp2/Eri3/Rpl10a/Rpl35a/Nop10/Rps24/Rpl14/Rps6/Rpl7/Rps17/Rpl35/Rpl27/Rps28/Rpl26/Rps15/Rps14
GO	peroxidase activity	8/733	31/11958	0.00042805	0.018807467	0.01810766	Hbb-bt/Txndc17/Hbb-bs/Hba-a2/Hba-a1/Gpx1/Mgst3/Gpx4
GO	translation factor activity, RNA binding	13/733	75/11958	0.000572984	0.02239819	0.021564777	Eif2b3/Cpeb4/Eif3b/Tufm/Eif6/Eif3f/Eif3g/Eif3h/Eif3i/Eif1b/Eif3k/Eef1g/Eif5a
GO	oxidoreductase activity, acting on NAD(P)H, quinone or similar compound as acceptor	7/733	25/11958	0.000573496	0.02239819	0.021564777	Ndufb7/Ndufs8/Ndufs7/Ndufa13/Ndufa7/Ndufa2/Ndufb8
GO	rRNA metabolic process	26/733	205/12053	0.000291587	0.024654642	0.024654642	Nop14/Nob1/Drosha/Smarca4/Gm9493/Rpl7l1/Emg1/Mrps11/Imp3/Exosc4/Nhp2/Eri3/Rpl10a/Rpl35a/Nop10/Rps24/Rpl14/Rps6/Rpl7/Rps17/Rpl35/Rpl27/Rps28/Rpl26/Rps15/Rps14
GO	organelle envelope lumen	12/755	75/12262	0.001970515	0.028676174	0.026091579	Coa4/Pnpt1/Triap1/Timm10b/Arl2/Timm10/Pink1/Ndufb7/Ndufa8/Timm8b/Chchd10/Chchd2
Reactome	Regulation of PTEN stability and activity	6/419	19/5985	0.001405692	0.033924043	0.03028404	Pten/Rps27a/Csnk2b/Stub1/Uba52/Ubb
GO	isomerase activity	17/733	120/11958	0.001004901	0.036107034	0.034763529	Hyi/Ppie/Yjefn3/Gstz1/Eci2/Tsta3/Itpk1/Ech1/Gm5160/Mcee/Pin1/Mpi/Ppib/Fkbp8/Gpi1/Tpi1/Ppia
GO	oxidoreductase activity, acting on peroxide as acceptor	8/733	35/11958	0.001027227	0.036107034	0.034763529	Hbb-bt/Txndc17/Hbb-bs/Hba-a2/Hba-a1/Gpx1/Mgst3/Gpx4
GO	mitochondrial proton-transporting ATP synthase complex	5/755	17/12262	0.002901727	0.04011638	0.036500675	Atp5e/Atp5k/Atp5g3/Atp5o/Atp5h
GO	proton-transporting ATP synthase complex	5/755	17/12262	0.002901727	0.04011638	0.036500675	Atp5e/Atp5k/Atp5g3/Atp5o/Atp5h
GO	autolysosome	4/755	11/12262	0.003319184	0.044768502	0.0407335	Map1lc3b/Ftl1/Map1lc3a/Fth1
GO	translation initiation factor activity	9/733	45/11958	0.001401886	0.046929817	0.045183608	Eif2b3/Eif3b/Eif6/Eif3f/Eif3g/Eif3h/Eif3i/Eif1b/Eif3k
GO	ATPase activity, coupled to transmembrane movement of ions, rotational mechanism	7/733	29/11958	0.001502565	0.048013776	0.046227234	Atp6v0e/Atp6v1f/Atp5e/Atp5g3/Atp5o/Atp6v0b/Atp5h